

# 18

## The $\lambda$ -measure in the leading-log and modified leading-log approximations of perturbative QCD

### 18.1 Introduction

We will in this chapter present the Lund model in a somewhat different and also more mathematical manner. We have already described the emergence of a string with the  $q$  and  $\bar{q}$  at the endpoints and with a set of color-connected gluonic excitations in the interior. This corresponds to a more or less complex string space-time surface, which via the directrix may be traced back to all these original excitations. The string breakup is then in Sjöstrand's version a process on the surface leading to a set of final-state (mostly) yoyo-like small hadron strings. All this is in accordance with the Lund model.

Since we have seen in the previous chapters how the string surface is obtained and how the string breaks up along the surface the reader should at this point learn how to use Lönnblad's program ARIADNE, which provides a kinematically precise implementation of the dipole cascade model, and then compare with the results of Webber's HERWIG or Sjöstrand's JETSET Monte Carlo simulation programs. In each case the reader will be able to produce an ensemble of partonic cascade excitations, corresponding to the chosen treatment of the way the color force field will be stretched.

After that either JETSET's or HERWIG's routines can be used (but when doing experimental analysis the reader is advised to use all available methods) to obtain the final-state fragmentation distributions stemming from the chosen ensemble. It is instructive to find for oneself that these seemingly very different approaches will in the end lead to very similar predictions for most inclusive distributions. It is a challenge to find particular differences which are amenable to experimental analysis and also to be able to trace these differences to the dynamical input in the models.

A rather different approach is also possible. Many people, in particular

theorists, want something more than just a Monte Carlo ‘black box’. It is the intention of this chapter to show that it is possible to calculate many observables in analytical approximations.

Although it is very satisfying to produce an analytical expression for an observable we should be aware that the approach is more approximate than the Monte Carlo methods because it is only partly possible to take the different kinematical constraints into account. To be frank the approximations which are necessary to obtain solvable analytical equations very often have the unfortunate property that the results may be misleading with respect to the dynamics.

But the fact that we generally deal with a multiparticle situation does imply some simplifications. As long as we only consider *inclusive* distributions then many of the approximations actually do not show up because they will drown in the general ‘noise’ in accordance with the laws of statistics and in particular the law of large numbers.

We will in general concentrate on the  $\lambda$ -measure, which was introduced in [48] to describe the multiplicity in complex multigluon situations. It constitutes a generalised rapidity variable and we described it in Chapter 15 in connection with the triangular phase space with its extended folds, which is typical of (multi)dipole emission. We will also discuss the distributions in the dipole multiplicity (which is related to the gluon multiplicity) but as expected this multiplicity is not, in contrast to the  $\lambda$ -measure, an infrared-stable quantity.

The intention is to introduce methods to calculate analytically *inclusive*  $\lambda$ -distributions. This means that we consider an ensemble of states, e.g. produced from a particular partonic cascade, and calculate the distribution in the variable  $\lambda$  over this ensemble. We will use two different methods, which we will refer to as the  $L$ -method and the  $\kappa$ -method.

In the  $L$ -method, [48] we consider the analytical equations which governs the change in the  $\lambda$ -distribution when we increase the energy, i.e. in particular increase the variable  $L = \log(s/s_0)$ . There are sudden and large changes in the distribution when we thus move upwards in virtuality. This is due to the fact that we then encounter very hard gluon radiation which means large changes in the states. The corresponding changes in the distribution have, however, a structure so that it is easy to describe the *Laplace-transformed distribution*. We derive a second-order differential equation for the Laplace-transformed distribution and we also show how to obtain the moments in  $\lambda$  directly from the differential equation.

This will lead us to the notion of KNO scaling [86] for the multiplicity distributions, although we will find that at this level of approximation we are rather far away, in the analytical formulas, from the observed distributions in  $e^+e^-$  annihilation events.

After that we turn to the  $\kappa$ -method, [6], where the idea is to consider

the production of new dipoles when we go downwards in the transverse momentum variable  $\kappa = \log(k_{\perp}^2/s_0)$  from a fixed maximum  $\kappa \simeq L$ . This leads to linear partial differential equations of a gain-loss character.

It is possible to investigate many local properties of the distribution in  $\lambda$  by means of this method. We will, however, concentrate more upon the complementarity of the two methods. We will in particular derive a kind of master equation for the combined distribution in  $\lambda$  and  $n_d$ , with  $n_d$  the number of dipoles for a given  $L$  and  $\kappa$ . From this equation it is easy to derive any kind of moment equation for the two variables.

Up to now we have used an approximation to perturbative QCD which is known as the *leading-log approximation*, the LLA. We will meet this approximation again in Chapter 19. It is rather easy to extend the approximation to the *modified leading-log approximation*, [52]. The basic point is to note that one loses a region close to the endpoints of every dipole, [72], in connection with the emission of particles. This is mostly due to recoil problems during the emission but is also related to the spin coupling between the emitters and the final-state partons. After we have taken these corrections into account we obtain quite good analytical approximations to the Monte Carlo simulated distributions in  $\lambda$  and  $n_d$ .

Owing to the similarity between the classical gain-loss equations and the Callan-Symanzik equations for the changes in the renormalisation point in a field theory we will at this point also speculate about the meaning of the running coupling constant in QCD.

We will after that present a very simple approximation scheme, called *discrete QCD* [15], which is based upon the properties of the coupling constant. It is possible in this scheme to exchange the continuous triangular phase space, which we have discussed repeatedly for the dipole emissions, for a lattice, where only a discrete set of emission points is available. Each emission point has a simple probability that there will be a gluon emission and a corresponding new triangular fold extended. Then the procedure of discretisation can again be extended to this triangle and later to the subtriangles etc. Therefore the whole structure corresponds to a 'tree' containing 'subtrees', 'branches' and 'twigs' etc. in accordance with simple prescriptions. The procedure leads to very good analytical approximations and also provides further insight into the structure of the perturbative QCD parton-branching processes.

Then we will consider the notion of *fractality* or rather *multi-fractality* in connection with QCD parton cascades. We start by presenting a method to visualise the average distributions of the final-state hadrons already from the partonic state by deriving an equation for a curve called the *x-curve* in [20] and [48].

The *x-curve* has an everywhere timelike tangent compared with the directrix curve, which is everywhere lightlike. Their relationship is that the

$x$ -curve is stretched along the hyperbolas which have the directrix curve as their asymptotes. The (invariant) length of the  $x$ -curve is equal to the measure  $\lambda$ , with  $\lambda$  this time defined in an infrared-stable way.

If the  $x$ -curve is cut up into pieces, each of a length corresponding to the mass of the final-state hadrons, then we recover the average energy-momentum distribution of the hadrons in accordance with the Lund model fragmentation process. In this way we have on the one hand derived the *local parton-hadron duality* concept in the Lund model, [53], and on the other hand presented a further way to visualise the relationship between the  $\lambda$ -measure and the final-state hadron multiplicity.

One may take the  $x$ -curve and its properties as the starting point for a fragmentation scheme, [21], in the spirit of the Lund model but with methods conceptually different from those in the Sjöstrand fragmentation scheme in Chapter 15. The idea is to find the variations around the  $x$ -curve from the Lund model fragmentation formulas. The final result is nevertheless similar to Sjöstrand's distributions but in this way we will be able to identify the transverse momentum correlation length, that was introduced in connection with the Ornstein-Uhlenbeck process in Chapter 12.

The curves under consideration in general do not exhibit simple regularity. If we go back to the phase-space triangle used to describe the emission region of gluons in Chapters 15 and 17, this statement is rather obvious. When we have drawn out its many folds from the gluon emissions it looks less like a smooth ordinary curve than one of the fractal curves which have been under intense investigation in recent years.

We will therefore investigate the dimensions of the curves we have derived from the point of view of such fractals. We will exhibit in some detail, [48], the fact that what has for a long time been known as the *anomalous dimensions of QCD* actually can be described also as the *(multi)fractal dimensions of the curves describing the  $\lambda$ -measure*.

## 18.2 The $L$ -method

### 1 The differential equations

We will in this section introduce a set of differential equations, [48], for the distribution in  $\lambda$  stemming from the dipole cascade model. In particular, we will investigate the changes in the  $\lambda$ -distribution with increasing energy. Then the phase-space triangle is increased in the upwards direction towards larger values of  $L = \log(s/s_0)$  (see Chapters 16 and 17 and Fig. 18.1). We will call the distribution in  $\lambda$  for a fixed value of  $L$ ,  $P(\lambda, L)$ .

We start by noticing that the size of the  $\lambda$ -measure obtains independent contributions from each particular  $y$ -region (usually called a  $y$ -bin). We

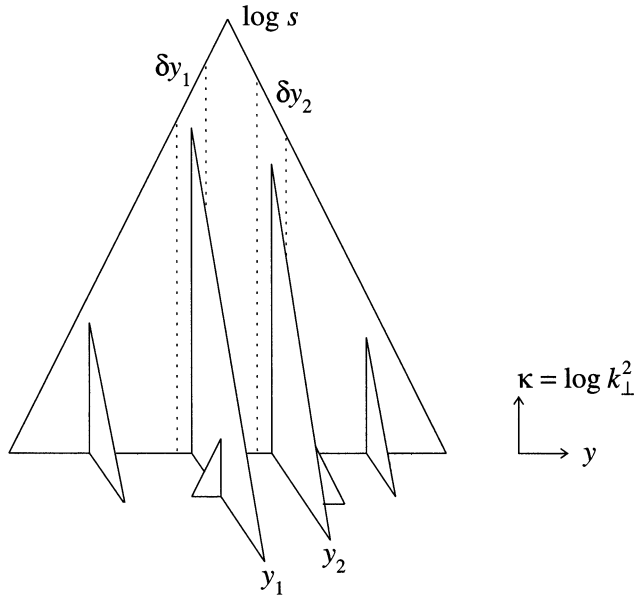


Fig. 18.1. The triangular phase space with the folds corresponding to new gluon emissions, with two independent regions in rapidity,  $\delta y_1$ ,  $\delta y_2$ , exhibited.

again stress the fact that neither  $k_{\perp}$ , and therefore  $\kappa$ , nor  $y$  necessarily correspond to directly observable momenta and rapidities. They are defined invariantly and recursively from the masses of the dipoles that arise.

The combined  $\lambda$ -distribution from the two regions, see Fig. 18.1,  $\delta y_1$  around  $y_1$  and  $\delta y_2$  around  $y_2$ , is then using  $P_j \equiv P_{\delta y_j}$  for the contributions from region  $j$ ,

$$P(\lambda; \delta y_1, y_1; \delta y_2, y_2) = \int P_1(\lambda_1)P_2(\lambda_2)d\lambda_1d\lambda_2\delta(\lambda_1 + \lambda_2 - \lambda) \quad (18.1)$$

Thus the folds which occur in a certain region are in this approximation independent of the folds in a different region. Therefore it is natural to go over to a Laplace transform of the distribution. Then we obtain by the definition

$$\tilde{P}(\beta, L) = \int d\lambda \exp(-\beta\lambda)P(\lambda, L) \quad (18.2)$$

the following result for the Laplace transform of Eq. (18.1):

$$\tilde{P}_{\delta y_1 + \delta y_2}(\beta) = \tilde{P}_{\delta y_1}(\beta)\tilde{P}_{\delta y_2}(\beta) \quad (18.3)$$

This implies that the logarithm of the distribution is additive (using

$\log \tilde{P}(\beta) \equiv \mathcal{L}(\beta)$ :

$$\mathcal{L}_{\delta y_1 + \delta y_2}(\beta) = \mathcal{L}_{\delta y_1}(\beta) + \mathcal{L}_{\delta y_2}(\beta) \tag{18.4}$$

It is then possible to define a function  $\mathcal{R}(\beta, y)$  corresponding to the limit of a vanishing  $\delta y$ -interval around a particular rapidity  $y$  within the phase space:

$$\mathcal{R}(\beta, y) = \lim_{\delta y \rightarrow 0} \frac{\mathcal{L}_{\delta y}(\beta, y)}{\delta y} \tag{18.5}$$

We may recover the distribution  $\mathcal{L}_{\Delta y}(\beta, y)$  for a finite  $\Delta y$ -interval by

$$\mathcal{L}_{\Delta y}(\beta, y) = \int_{y-\Delta y/2}^{y+\Delta y/2} \mathcal{R}(\beta, y') dy' \tag{18.6}$$

We next remark that for a given  $y$  the distribution  $\mathcal{R}(\beta, y)$  can only depend upon the maximum value of the (logarithmic) squared  $k_{\perp}$  that can occur for that  $y$ -value. We will denote as  $\ell(y)$ , the variable  $\log(k_{\perp, \max}^2/s_0)$  for a given  $y$  and we obtain from the triangular phase space the equality  $\ell(y) = L - 2|y|$ . It is then possible to write the following formula for  $\mathcal{L}(\beta, L)$ , the distribution for the total  $L$ -region:

$$\mathcal{L}(\beta, L) = \int_{-L/2}^{L/2} dy \mathcal{R}(\beta, \ell = L - 2|y|) = \int_0^L d\ell \mathcal{R}(\beta, \ell) \tag{18.7}$$

We will now consider the change in  $\mathcal{R}$  when  $\ell \rightarrow \ell + \delta$  and concentrate upon a particular infinitesimal  $y$ -region  $\Delta$  around  $y$ . There is the probability

$$\Delta \delta \frac{\alpha_0}{\ell} \tag{18.8}$$

of obtaining a new gluon inside the region which is shaded in Fig. 18.2. If there is such a gluon then the increase in  $\lambda$  is described by  $P(\lambda, \ell(y))$ , because with all its folds and subfolds it corresponds exactly to an isolated system with  $L = \ell(y)$ . In Eq. (18.8) we have introduced the running coupling constant of QCD,  $3\alpha_s k_{\perp, \max}^2 / (2\pi) \equiv \alpha_0 / l$ . This means that we have identified the scale  $s_0 = \Lambda_{QCD}^2$ .

The remaining probability  $1 - \Delta \delta \alpha_0 / \ell$  corresponds to the case when there is no extra gluon and consequently  $\lambda$  is unchanged. We obtain

$$P_{\Delta}(\lambda, \ell + \delta) = (1 - \Delta \delta \frac{\alpha_0}{\ell}) P_{\Delta}(\lambda, \ell) + \Delta \delta \frac{\alpha_0}{\ell} \int d\lambda_1 d\lambda_2 P_{\Delta}(\lambda_1, \ell) P(\lambda_2, \ell(y)) \delta(\lambda_1 + \lambda_2 - \lambda) \tag{18.9}$$

We may now subtract  $P_{\Delta}(\lambda, \ell)$  from both sides, take the Laplace transforms and go to the limit  $\delta, \Delta \rightarrow 0$  to obtain the following result for  $\mathcal{R}$ :

$$\frac{d\mathcal{R}(\beta, \ell)}{d\ell} = \frac{\alpha_0}{\ell} [\exp \mathcal{L}(\beta, \ell) - 1] \tag{18.10}$$

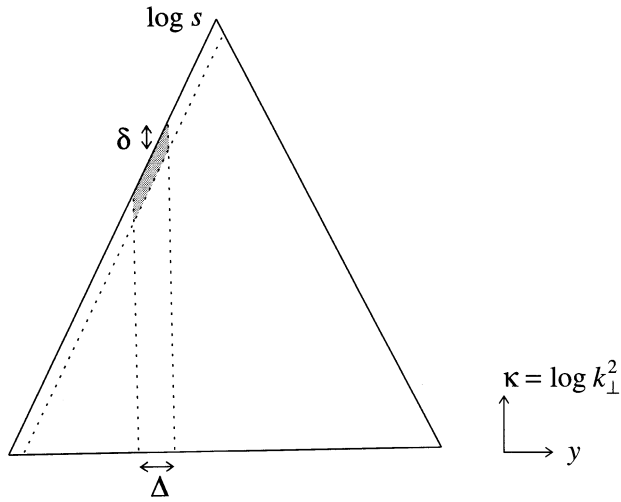


Fig. 18.2. The region for emitting a gluon obtained by increasing  $L$  and thereby also the local  $\ell$  is shown as shaded.

Combining this equation with the result in Eq. (18.7) we obtain the second order differential equation

$$\frac{d^2 \mathcal{L}(\beta, \ell)}{d\ell^2} = \frac{\alpha_0}{\ell} [\exp \mathcal{L}(\beta, \ell) - 1] \tag{18.11}$$

In order to specify the function  $\mathcal{L}(\beta, L)$  we must supplement Eq. (18.11) with the proper boundary conditions. For  $L = 0$  we evidently have a  $\delta$ -contribution, i.e.  $P(\lambda, 0) = \delta(\lambda)$ , which implies that  $\mathcal{L}(\beta, 0) = 0$ . Further for small values of  $L$  the contributions to  $\lambda$  from the gluons is of order  $L^2$ . This means that  $d\mathcal{L}(\beta, 0)/dL = -\beta$ .

### 2 The moments in $\lambda$

Equation (18.11) with these boundary conditions has unfortunately no solution in terms of elementary functions. Numerical solutions of Eq. (18.11) indicate that a good approximation for the distribution  $P(\lambda, L)$  is given by a  $\Gamma$ -distribution:

$$P(\lambda, L) \simeq \frac{\lambda^{\nu-1} \rho^\nu}{\Gamma(\nu)} \exp(-\rho\lambda) \tag{18.12}$$

where  $\nu$  and  $\rho$  are slowly varying functions of  $\alpha_0 L$ . For large values of  $L$  the result in Eq. (18.29) implies that  $\nu \rightarrow 3$ . This estimate is, however, due to kinematical corrections rather bad and should be exchanged for

$v \sim 7-8$  at all present and foreseeable energies, although the general shape is reasonable according to [74].

In order to relate the distribution to the observables we assume that for a given value of  $\lambda$  there is, besides the distribution in  $\lambda$  for given  $s$  which we have considered above, a definite multiplicity distribution of final-state hadrons  $P(n, \lambda)$ , independent of the energy:

$$P_{tot}(n, s) = \int d\lambda P(\lambda, s)P(n, \lambda) \quad (18.13)$$

This assumption is very well fulfilled according to the simulations with ARIADNE (to produce the  $\lambda$ -distribution) and JETSET (to produce the fragmentation). The distribution  $P(n, \lambda)$  is then close to a Poissonian with the average multiplicity for fixed  $\lambda$ ,  $\langle n \rangle(\lambda) = m\lambda$ , where  $m$  is a constant.

Although we cannot calculate the distribution itself it is nevertheless possible to calculate the moments of the  $\lambda$ -distribution,

$$\langle \lambda^n \rangle = \int d\lambda \lambda^n P(\lambda, L) \quad (18.14)$$

directly from the differential equation.

Thus we have from the defining equation of the Laplace transform

$$\begin{aligned} \exp(\mathcal{L}(\beta, L) \equiv \tilde{P}(\beta, L) &= \int d\lambda \exp(-\beta\lambda)P(\lambda, L) \\ &= \sum_{j=0}^{\infty} \frac{(-\beta)^j}{(j)!} \int d\lambda \lambda^j P(\lambda, L) \end{aligned} \quad (18.15)$$

It is straightforward to prove for the first two moments, the mean  $\langle \lambda \rangle$  and the variance  $V_\lambda = \langle \lambda^2 \rangle - \langle \lambda \rangle^2$ , that if

$$\mathcal{L}(\beta, L) = -\beta G_1(L) + \beta^2 G_2(L) + O(\beta^3) \quad (18.16)$$

then

$$\begin{aligned} \langle \lambda \rangle &= G_1(L) \\ V_\lambda \equiv \langle \lambda^2 \rangle - \langle \lambda \rangle^2 &= \langle (\lambda - \langle \lambda \rangle)^2 \rangle = 2G_2(L) \end{aligned} \quad (18.17)$$

The differential equation for  $G_1$  is immediately obtained from the first-order expansion in  $\beta$  of Eq. (18.11):

$$\frac{d^2 G_1}{dL^2} = \frac{\alpha_0}{L} G_1 \quad (18.18)$$

(It is worthwhile to go through the calculations leading to Eqs. (18.15)–(18.18).)

The solutions to this equation are related to the modified Bessel functions of first rank,  $I_j$  and  $K_j$ . As we are going to use these solutions

repeatedly we will introduce a special notation for them:

$$\mathcal{I}_1(\kappa) = \sqrt{2\kappa}I_1(2\sqrt{\alpha_0\kappa}), \quad \mathcal{I}_0(\kappa) = \sqrt{2\alpha_0}I_0(2\sqrt{\alpha_0\kappa}) \quad (18.19)$$

with similar relations between  $\mathcal{K}_j$  and  $K_j$ . These functions fulfil

$$\frac{d\mathcal{I}_1}{d\kappa}(\kappa) = \mathcal{I}_0(\kappa), \quad \frac{d\mathcal{I}_0}{d\kappa}(\kappa) = \frac{\alpha_0}{\kappa}\mathcal{I}_1(\kappa) \quad (18.20)$$

with similar relations for  $\mathcal{K}_j$  but with a negative sign. The functions are normalised so that

$$\mathcal{I}_1\mathcal{K}_0 + \mathcal{K}_1\mathcal{I}_0 = 1 \quad (18.21)$$

We also note the limiting behaviour

$$\begin{aligned} \lim_{\kappa \rightarrow 0} \mathcal{K}_1(\kappa) &= \frac{1}{\sqrt{2\alpha_0}} \\ \lim_{L \rightarrow \infty} \mathcal{I}_1(L) &= \frac{L^{1/4}}{(2\pi)^{1/2}\alpha_0^{1/4}} \exp(2\sqrt{\alpha_0 L}) \\ \lim_{L \rightarrow \infty} \mathcal{K}_1(L) &= \frac{\pi^{1/2}L^{1/4}}{2^{1/2}\alpha_0^{1/4}} \exp(-2\sqrt{\alpha_0 L}) \end{aligned} \quad (18.22)$$

All these relations are easy to prove from any handbook on Bessel functions, e.g. [57]. It can also be seen from a combination of Eqs. (18.20) that the general solution to Eq. (18.18) is a linear combination of  $\mathcal{I}_1$  and  $\mathcal{K}_1$ ,

$$G_1 = A\mathcal{I}_1 + B\mathcal{K}_1 \quad (18.23)$$

where the numbers  $A$  and  $B$  must be chosen so that the boundary conditions are fulfilled. Thus  $G_1 = 0$  and  $dG_1/dL = 1$  at the starting point, according to the boundary conditions for Eq. (18.11). We will choose the starting point to be a bit more general than before,  $L = L_0$ , and assume that  $L_0$  may be different from 0.

It is then easy to prove by means of the relations in Eqs. (18.20), (18.21) and (18.22) that the general solution is

$$\begin{aligned} G_1(L, L_0) &= \mathcal{I}_1(L)\mathcal{K}_1(L_0) - \mathcal{K}_1(L)\mathcal{I}_1(L_0) \\ &\rightarrow \frac{(LL_0)^{1/4}}{2(\alpha_0)^{1/2}} \exp[2(\sqrt{\alpha_0 L} - \sqrt{\alpha_0 L_0})] \\ G_1(L, 0) &= \sqrt{\frac{L}{\alpha_0}}I_1(2\sqrt{\alpha_0 L}) \rightarrow \sqrt{\frac{L^{1/2}}{\alpha_0^{3/2}4\pi}} \exp(2\sqrt{\alpha_0 L}) \end{aligned} \quad (18.24)$$

where the limits correspond to  $L \gg L_0 \gg 0$ .

The corresponding differential equation for the variance in  $\lambda$  is obtained

from the expansion coefficient proportional to  $\beta^2$  in Eq. (18.11):

$$\frac{d^2 G_2}{dL^2} = \frac{\alpha_0}{L} \left( G_2 + \frac{G_1^2}{2} \right) \quad (18.25)$$

with the condition that  $G_2 = dG_2/dL = 0$  at the starting point. The equation can then be easily solved by means of the Green's function method, i.e. we look for a solution to the equation

$$\frac{d^2 G}{dL^2} - \frac{\alpha_0}{L} G = \delta(L - L') \quad (18.26)$$

with the same boundary values as for  $G_2$ . This is obtained by the use of  $G_1$  from Eq. (18.24) above:

$$G(L, L') = \Theta(L - L') \frac{G_1(L, L')}{2} \quad (18.27)$$

In this way we obtain the following result for  $G_2$ :

$$G_2(L, L_0) = \frac{1}{4} \int_{L_0}^L \frac{\alpha_0}{L'} G_1(L, L') dL' G_1^2(L', L_0) \quad (18.28)$$

We obtain using the asymptotic expression for  $G_1 = \langle \lambda \rangle$

$$V_\lambda \rightarrow \frac{\langle \lambda \rangle^2}{3} \quad (18.29)$$

The reader is once again invited to carry through the necessary calculations to prove Eqs. (18.24)–(18.29).

### 3 *The notion of KNO scaling and the fact that the dipole cascade is dominated by the first two gluon emissions*

The result that the variance in the multiplicity of final-state particles obeys  $V_n \simeq C_2 \langle n \rangle^2$  has been known for a long time in high-energy physics. It was first known as the Wroblewski relation and later extended to the notion of KNO scaling, [86]. It was then applied to hadronic reactions but it is nowadays known that both  $e^+e^-$  annihilation and inelastic lepto-production event multiplicities exhibit a similar structure.

The basic idea in KNO scaling is that the multiplicity distributions,  $P(n, s)$ , scale with the mean multiplicity. For a squared cms energy  $s$  the suggestion is that

$$P(n, s) = \frac{1}{\langle n \rangle (s)} F \left( \frac{n}{\langle n \rangle (s)} \right) \quad (18.30)$$

where  $\langle n \rangle (s)$  is the mean multiplicity at the squared cms energy  $s$  and  $F$  a continuous function which depends upon the dynamics of the particular

interaction but is independent of the energy. It is then evident that all moments  $\langle n^j \rangle$ , not only the second one, will be proportional to  $\langle n \rangle^j$ .

There are some problems to be faced in connection with the approximation of a discrete distribution in terms of a continuous function. Different investigators have therefore used somewhat different ways to define the relationship between  $F$  and  $P_n$ . One reason is that if we consider e.g. a proton-proton reaction and concentrate on the charged particles then charge conservation means that only particle pairs with one positive and one negative can be produced. Therefore it is only possible to observe an even number of charged particles. Further it is not known whether the particles carrying the original two positive charges should be included. One solution would be to define the variable  $x$  as  $x = (n - n_0) / (\langle n \rangle - n_1)$ , where  $n_0, n_1$  are suitably chosen parameters for the argument in  $F(x)$ .

Nevertheless, Eq. (18.30) gives, if you allow for these uncertainties, a surprisingly good description of a large amount of multiplicity data from many different processes and energies. The function  $F$  is, however, process dependent.

There have been many speculations on the origin of the KNO scaling property. We will be satisfied with a few comments. Suppose that the basic particle-production mechanism corresponds to truly independent production as in the case of an external current acting on the different frequencies of a quantum field (the Schwinger model in Chapter 3). There are reasons for such a simple assumption. Multiparticle production generally leads to a flat central rapidity distribution without much correlation between the produced particles. Then it would be pure chance whether there is an observed particle in a small rapidity bin or whether it will be empty. This would, however, imply Poissonian statistics (just as we obtained for the external current). Therefore one should expect that the variance behaves as  $V_n \propto \langle n \rangle$  instead of the KNO prediction. Consequently it is necessary to introduce more dynamical assumptions to obtain the wider KNO scaling distributions.

There is a set of necessary constraints on particle production in both the Lund model and other successful models. The total charge and energy-momentum must be conserved during the production process. Further there is resonance production, which will introduce local correlations in rapidity because the decay products are spread over 1–2 units in rapidity. All such phenomena can be accounted for within the simpler schemes used in the iterative cascade models, which were described in Chapters 7 and 9. In general these models predict, nevertheless, an essentially Poissonian statistics for the central production in rapidity. The breakup of a single Lund  $q\bar{q}$ -string also leads to something close to a Poissonian (although a somewhat narrower, cf. the treatment of the Feynman-Wilson gas in Chapter 11). It should, however, be understood that for small energies

the fragmentation distributions are wider than Poissonian because then the phase space is dominated by the regions close to the string endpoints where the variations are larger.

If several different production processes *independently* contribute to the final hadronic state then the total multiplicity distribution will be a folding of the different distributions. In this case it is easy to prove that the variance will be simply additive, and there will not be much widening from such an assumption unless one distribution is very wide by itself,

$$P_{tot}(n) = \sum_{n_1+\dots+n_N=n} P_1(n_1) \cdots P_N(n_N) \quad (18.31)$$

$$\langle \sum n_j \rangle = \sum \langle n_j \rangle, \quad V(\sum n_j) = \sum V_{n_j}$$

It is, however, rather easy to obtain a broad distribution if there are several contributing processes *which exclude each other*. If we have two processes,  $j = 1, 2$ , with the probabilities  $\alpha$  and  $1 - \alpha$  occurring we have for the total multiplicity distribution and its moments

$$P_{tot}(n) = \alpha P_1(n) + (1 - \alpha) P_2(n)$$

$$\langle n \rangle_{tot} = \alpha \langle n \rangle_1 + (1 - \alpha) \langle n \rangle_2 \quad (18.32)$$

$$V(n_{tot}) = \alpha V_1 + (1 - \alpha) V_2 + \alpha(1 - \alpha)(\langle n \rangle_1 - \langle n \rangle_2)^2$$

This is much broader than each of the distributions when the mean multiplicities are different in the two processes. In hadronic interaction models this is often used to explain KNO scaling because in this case there are, besides a general smooth central production, also *diffractive events* with smaller multiplicities concentrated around the incoming particle rapidities.

For hard QCD processes it is instead the bremsstrahlung of gluons which causes the broadening of the multiplicity distributions. This means that it is the folding in Eq. (18.13) which is responsible and there is a large width in the  $\lambda$ -distribution in accordance with what we have learned; this should be compared to the statement in Eq. (18.31).

The Lund model predicts, in good agreement with data, a KNO scaling result. This stems from a combination of the fragmentation process and the partonic cascade. Using the results from Eq. (18.13) we obtain

$$\langle n \rangle_{tot}(s) = m \langle \lambda \rangle(s) = \langle n \rangle(\lambda = \langle \lambda \rangle(s)) \quad (18.33)$$

$$V_{tot} = m^2 V_\lambda(s) + V_n(\lambda = \langle \lambda \rangle(s)) \equiv V_{casc} + V_{frag}$$

In this way we have partitioned the variance into the cascade contribution, i.e. the variations in  $\lambda$  for fixed  $s$ , and the fragmentation contribution, the variations in multiplicity for a fixed generalised rapidity region  $\lambda$ . We can go further and obtain two independent contributions to the (squared)

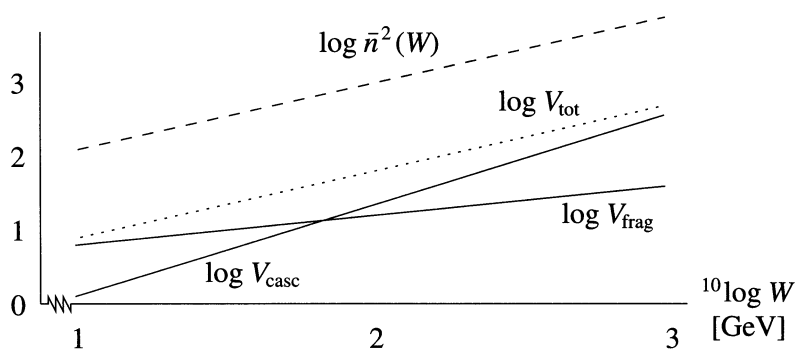


Fig. 18.3. The contributions to the multiplicity variance stemming from the dipole cascade model (ARIADNE for  $\lambda$ ) and from the Lund fragmentation model (JETSET), together with the total variance (dotted line) and the square of the mean multiplicity (broken line). The variable  $W$  is the square root of  $s$ .

width over the mean:

$$\frac{V_{tot}}{\langle n \rangle_{tot}^2} = \frac{V_\lambda}{\langle \lambda \rangle^2} + \frac{V_n(\lambda = \langle \lambda \rangle(s))}{\langle n \rangle^2(\lambda = \langle \lambda \rangle(s))} \tag{18.34}$$

The resulting distribution is shown in Fig. 18.3. While the contributions lead to a smooth, almost constant, ratio, one of them, the fragmentation contribution, dominates at small values of  $s$  and the other, the cascade contribution, dominates for large  $s$ . The crossing point is somewhere below the LEP energies.

We end this section with another result from the investigations of the dipole cascade model. *It is possible to show that almost all the variations in the  $\lambda$ -distribution stem from the emission of the first two gluons.*

To understand this result we will make use of the distributions  $\mathcal{R}$  and  $\tilde{\mathcal{P}} = \exp \mathcal{L}$ , which are defined in Section 1. They correspond to particular Laplace transforms of the  $\lambda$ -distribution.

We assume that the first gluon (i.e. the one with the largest  $k_\perp$ ) is emitted at  $\log(k_{\perp 1}^2/s_0) = \kappa_1$ . From Fig. 18.4 we obtain that the total  $\mathcal{L}$ -distribution for these kind of events,  $\mathcal{L}(\beta, L, \kappa_1)$ , is given by

$$\mathcal{L}(\beta, L, \kappa_1) = 2\mathcal{L}(\beta, \kappa_1) + (L - \kappa_1)\mathcal{R}(\beta, \kappa_1) \tag{18.35}$$

The first contribution on the right-hand side stems from the two half-triangles at the outskirts and the folded triangle from the emission at  $\kappa_1$ . The rest stems from what is left of the background triangle, i.e. the rectangle with side length  $L - \kappa_1$ . Therefore the average and the variance in  $\lambda$  (the two lowest-order power contributions in  $\beta$ ) are remembering that

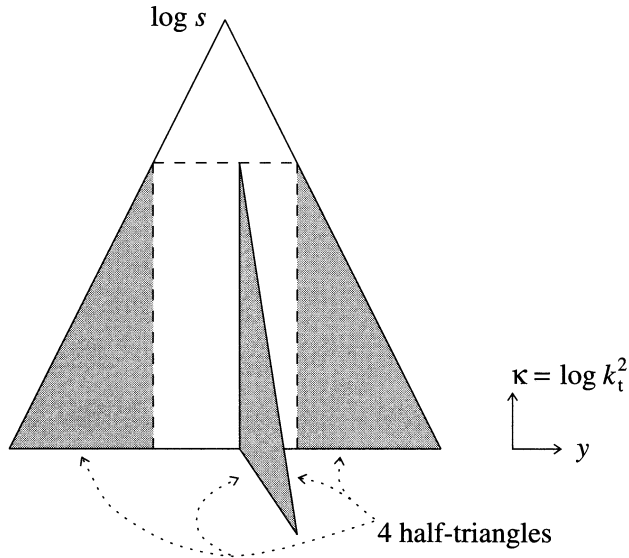


Fig. 18.4. The emission of the first and hardest gluon partitions the remainder of the  $\lambda$ -distribution for such states into one contribution from the  $\mathcal{R}$ , integrated over the centre, and the contributions from two triangular regions, one along the two boundaries and one from the gluon fold.

$\mathcal{R}$  is the derivative of  $\mathcal{L}$ ,

$$\begin{aligned} \langle \lambda \rangle (L, \kappa_1) &= 2 \langle \lambda \rangle (\kappa_1) + (L - \kappa_1) \frac{d}{d\kappa_1} \langle \lambda \rangle (\kappa_1) \\ V_\lambda(L, \kappa_1) &= 2V_\lambda(\kappa_1) + (L - \kappa_1) \frac{d}{d\kappa_1} V_\lambda(\kappa_1) \end{aligned} \tag{18.36}$$

The total variance for a given  $L$ ,  $V_{tot}(L)$ , stems from the variations in the first emission together with the variations of all the remaining gluons, averaged over the first emission. To calculate the variation in  $\kappa_1$  we must as always introduce a Sudakov factor  $f$ , corresponding to no emission before  $\kappa_1$ ,

$$\begin{aligned} V_{tot}(L) &= \left\{ \int d\kappa_1 f(\kappa_1) \langle \lambda \rangle^2 (L, \kappa_1) - \left( \int d\kappa_1 f(\kappa_1) \langle \lambda \rangle (L, \kappa_1) \right)^2 \right\} \\ &\quad + \int d\kappa_1 f(\kappa_1) V_\lambda(L, \kappa_1) \end{aligned} \tag{18.37}$$

From the bremsstrahlung cross section we obtain, integrating over the

available rapidity range with  $3\alpha_s/2\pi = \alpha_0/\kappa$ ,

$$\frac{dn_g}{d\kappa_1} = \frac{\alpha_0}{\kappa_1}(L - \kappa_1) \quad (18.38)$$

Then if  $(L - \kappa_1)/L \ll 1$ ,  $f$  will asymptotically behave as a gaussian distribution:

$$f \simeq \alpha_0 \frac{L - \kappa_1}{L} \exp \left[ -\frac{\alpha_0(L - \kappa_1)^2}{2L} \right] \quad (18.39)$$

It is then rather easy to introduce the results for  $V_\lambda(L, \kappa_1)$  and  $f$  to perform the second integral in Eq. (18.37). We obtain an error-function result which is equal to

$$\int d\kappa_1 f(\kappa_1) V_\lambda(L, \kappa_1) \simeq 0.53 V_{tot}(L) \quad (18.40)$$

From this approximation we obtain that the variations from the first gluon emission in this asymptotic scenario contribute around 47% to the total variance.

It is possible to do the same calculation for the second, third etc. gluons and it is also possible to simulate the variations from ARIADNE in the way described in [12]. We find that over the PETRA-PEP energy range around 95% of the variance stems from the variations in the first gluon emission. Over the LEP-SLC region more than 87% of the variance stems from the first and in total more than 95% from the first two gluon emissions.

The reason for this result is that if we have a hard gluon emission  $\kappa_1 \sim L$  we obtain a very different kind of event as compared to the case when  $\kappa_1 \ll L$ . In both cases there will be further gluon emissions but the variations in them will at the present energies give very small contributions to the variations in the final-state multiplicities.

We are basically invoking the *very slow development of the QCD cascades* and we will come back to this later on. But even the asymptotic result, i.e. that for all energies around half of the variations stem from the first gluon, is quite surprising!

## 18.3 The $\kappa$ -method

### 1 Preliminaries

There is one inconvenient property of the  $L$ -method and that is that when we search the phase space for gluon emissions upwards, i.e. for increasing  $L$ , we obtain hard gluon contributions to the  $\lambda$ -distribution. This means that the  $L$ -method leads to discontinuous changes in  $\lambda$ . But the structure

of independence in the  $y$ -variable means that the Laplace-transformed  $\lambda$ -distributions change in a smooth and differentiable way.

We will now introduce a different method, [6], in which for a fixed value of  $L$  we go downwards in  $\kappa$  in the phase space, looking for gluons with smaller and smaller  $k_{\perp}$ . In this way we obtain a smooth and differentiable distribution in the dipole productions and thereby also in  $\lambda$ .

The basic idea is to introduce the *notion of virtual dipole size at the level*  $\kappa$ , to be called  $\mu$  for an individual dipole. We define the variable  $\mu$  for a dipole of squared mass  $s_d$  as the rapidity size within which the dipole can emit gluons with transverse momentum  $k_{\perp}$  (cf. the triangular phase space size)

$$\mu = \log(s_d/s_0) - \log(k_{\perp}^2/s_0) \equiv L_d - \kappa \quad (18.41)$$

In order to see the general behaviour we will firstly study the (inclusive) distribution in the  $\mu$ -variable for the dipole containing the original  $q$ -particle (the right-endpoint dipole), to be called  $P_1(\mu, \kappa)$ . For simplicity we suppress the dependence on the starting point of the evolution,  $\kappa_{max}$ .

We now show how to write gain-loss equations for the distribution  $P_1$  when we change the *resolution scale*  $\kappa$ . We firstly note that the dipole size  $\mu$  will obviously due to its definition increase to  $\mu + \delta\kappa$  when we decrease  $\kappa$  to  $\kappa - \delta\kappa$ .

A dipole of size  $\mu$  may, however, also split up into two dipoles,  $\mu_1$  and  $\mu_2$ , when  $\kappa \rightarrow \kappa - \delta\kappa$ . The probability for this to happen is

$$\frac{\alpha_0}{\kappa} \delta\kappa d\mu_1 d\mu_2 \delta(\mu - \mu_1 - \mu_2) \quad (18.42)$$

This is a rewriting of the ordinary cross section for gluon emission, once again with the effective running coupling  $3\alpha_s/2\pi \equiv \alpha_0/\kappa$ . We have assumed that there is in the dipole rest frame a rapidity value  $y$  such that  $|y| \leq \mu/2$  and that a new gluon is emitted at  $(\kappa, y)$ . Thus the dipole is split into two with virtual sizes  $\mu/2 \pm y$ ; these are called  $\mu_1$  and  $\mu_2$  in Eq. (18.42).

After the splitting each new dipole will increase independently of the other one when we go downwards in the cascade, according to the basic assumption of the DCM. These dipole sizes correspond to the available emission hyperbolas from the endpoints of the  $\mu$ -dipole, via the new gluon 'peak', according to the description in Chapter 15.

## 2 The distribution of the endpoint dipole

The distribution  $P_1$  can thus change in three ways when we take the step  $\kappa \rightarrow \kappa - \delta\kappa$ :

- 1 The value of  $\mu$  at  $\kappa - \delta\kappa$  may correspond to the value  $\mu - \delta\kappa$  at  $\kappa$ .

- 2 It is possible for a dipole of size  $\mu$  to decay into smaller-size dipoles according to Eq. (18.42) (loss at the value  $\mu$ ).
- 3 It is possible that a larger dipole  $\mu_1 > \mu$  will decay into  $\mu$  according to Eq. (18.42) (gain at the value  $\mu$ ).

Gathering these contributions we obtain the following partial differential equation, using the effective coupling  $\bar{\alpha} = \alpha_0/\kappa$ ,

$$\frac{\partial P_1}{\partial \kappa} - \frac{\partial P_1}{\partial \mu} \equiv \Delta_1 P_1 = \frac{\alpha_0}{\kappa} \left( \mu P_1 - \int_{\mu} d\mu_1 P_1(\mu_1, \kappa) \right) \tag{18.43}$$

The distribution  $P_1$  should obviously be normalised to 1 for all  $\kappa$ , so that we have

$$N_{1j}(\mu, \kappa) = \int_{\mu} d\mu_1 (\mu_1)^{j-1} P_1(\mu_1, \kappa), \quad N_{11}(0, \kappa) = 1 \tag{18.44}$$

If we perform a partial integration in  $\mu$  on the integro-differential equation in Eq. (18.43) we obtain a partial differential equation solely in  $N_{11}$ :

$$\Delta_1 N_{11} = \frac{\alpha_0}{\kappa} \mu N_{11} \tag{18.45}$$

We note the similarity to the Callan-Symanzik equation which was treated in Chapter 4. We will again solve it by integration along rays:

$$\frac{d\mu}{d\kappa} = -1 \quad \Rightarrow \quad C_1 = \mu + \kappa \tag{18.46}$$

where  $C_1$  is a constant. We obtain including the right boundary condition

$$N_{11}(\mu, \kappa) = \Theta(L - \mu - \kappa) \exp \left( - \int_{\kappa}^{\mu+\kappa} dy (\mu + \kappa - y) \alpha_0 / y \right) \tag{18.47}$$

The step function corresponds to the largest value the ray parameter  $C_1$  can take on, i.e. the starting point of the cascade,  $L$ . The distribution  $P_1$  obviously fulfils

$$P_1 = - \frac{\partial N_{11}}{\partial \mu} \tag{18.48}$$

and therefore contains a  $\delta$ -distribution corresponding to the situation when there has been no gluon emission and we are left with the original dipole of size  $\mu = L - \kappa$  at this virtuality. The coefficient in front of the  $\delta$ -distribution is the Sudakov exponential factor, which was approximated by means of a gaussian in connection with Eq. (18.39):

$$f_{Sud}(L, \kappa) = \exp \left( - \int_{\kappa}^L dy (L - y) \alpha_0 / y \right) \tag{18.49}$$

3 The general inclusive single-dipole distribution

In this subsection we will be concerned with the inclusive distribution  $\mathcal{P}_1$  for all the available dipoles whether they are endpoint dipoles or central ones. There are then two differences compared to  $P_1$ . The first one is related to the normalisation. If we define

$$\mathcal{N}_{1j}(\mu, \kappa) = \int_{\mu} d\mu_1 \mu_1^{j-1} \mathcal{P}_1(\mu_1, \kappa) \tag{18.50}$$

then  $\mathcal{N}_{11}(0, \kappa) \equiv M_1(\kappa)$  corresponds to the average number of dipoles at the virtuality  $\kappa$ . In the same way  $\mathcal{N}_{12}(0, \kappa) \equiv M_2(\kappa)$  corresponds to the total length of these dipoles, which evidently must be identical to the average  $\langle \lambda \rangle$ , defined before.

The second difference is the fact that the gain factor from the decays of larger dipoles is 2 instead of 1 because each dipole of length  $\mu_1 > \mu$  will decay into two dipoles and either one of them may have the length  $\mu$ . Thus the integro-differential equation (18.43) becomes

$$\Delta_1 \mathcal{P}_1 = \frac{\alpha_0}{\kappa} \left[ \mu \mathcal{P}_1 - 2 \int_{\mu} d\mu_1 \mathcal{P}_1(\mu_1, \kappa) \right] \tag{18.51}$$

These changes mean that if we again perform a partial integration in  $\mu$  we obtain instead of a single equation a set of two coupled partial differential equations from Eq. (18.51) for the first two moments of  $\mathcal{P}_1$ :

$$\Delta_1 \mathcal{N}_{11} = -\frac{\alpha_0}{\kappa} (\mathcal{N}_{12} - 2\mu \mathcal{N}_{11}), \quad \Delta_1 \mathcal{N}_{12} = -\mathcal{N}_{11} + \frac{\alpha_0}{\kappa} \mu^2 \mathcal{N}_{11} \tag{18.52}$$

From these equations we immediately obtain for the quantities  $M_j, j = 1, 2$ , which are defined above,

$$\frac{dM_1}{d\kappa} = -\frac{\alpha_0}{\kappa} M_2, \quad \frac{dM_2}{d\kappa} = -M_1 \tag{18.53}$$

If we combine these two equations we obtain back the second-order equation already derived for  $M_2 \equiv \langle \lambda \rangle$  before (Eq. (18.18)),

$$\frac{d^2 M_2}{d\kappa^2} = \frac{\alpha_0}{\kappa} M_2 \tag{18.54}$$

and the solution is the same (cf. Eq. (18.24)):

$$M_2(L, \kappa) = \mathcal{I}_1(L) \mathcal{K}_1(\kappa) - \mathcal{K}_1(L) \mathcal{I}_1(\kappa) \tag{18.55}$$

The second equation in (18.53) tells us that the mean number of dipoles is given by the (negative)  $\kappa$ -derivative of  $\langle \lambda \rangle$ :

$$\langle n_d \rangle = \mathcal{I}_1(L) \mathcal{K}_0(\kappa) + \mathcal{K}_1(L) \mathcal{I}_0(\kappa) \equiv M_1(L, \kappa) \tag{18.56}$$

From the properties of Eq. (18.21) we conclude that  $M_1(L, L) = 1$  while  $M_2(L, L) = 0$ . It is a very general property of second-order differential

equations that we can find another pair of functions  $M_3$  and  $M_0$  which also fulfils Eqs. (18.53) with  $M_3 \rightarrow M_2$  and  $M_0 \rightarrow M_1$ :

$$\begin{aligned} M_3(L, \kappa) &= \mathcal{I}_0(L)\mathcal{K}_1(\kappa) + \mathcal{K}_0(L)\mathcal{I}_1(\kappa) \\ M_0(L, \kappa) &= \mathcal{I}_0(L)\mathcal{K}_0(\kappa) - \mathcal{K}_0(L)\mathcal{I}_0(\kappa) \end{aligned} \tag{18.57}$$

This time the pair fulfils  $M_3(L, L) = 1$  and  $M_0(L, L) = 0$ . Using the two pairs of solutions it is possible to write out the mean of the  $\lambda$  and the number of dipoles  $n_d$  in the general situation when we take the ensemble of states which starts at  $L = \ell_0$  with  $\lambda = \lambda_0$  and  $n_d = n_{d0}$ :

$$\begin{aligned} \langle \lambda \rangle (\ell_0, \kappa) &= n_{d0}M_2(\ell_0, \kappa) + \lambda_0M_3(\ell_0, \kappa) \\ \langle n_d \rangle (\ell_0, \kappa) &= n_{d0}M_1(\ell_0, \kappa) + \lambda_0M_0(\ell_0, \kappa) \end{aligned} \tag{18.58}$$

We will meet all these functions later in a more general context but it is worthwhile to convince oneself that Eqs. (18.57) and (18.58) are correct.

While the mean value of  $\lambda$  (in both the cases discussed above) is finite also when  $\kappa \rightarrow 0$  (cf. Eq. (18.24)) we find that the mean number of dipoles diverges logarithmically in that limit.

#### 4 An aside on the rate of decay in QCD cascades

In this subsection we will give a simple explanation for the results in Eqs. (18.24) and (18.56) in order to understand the way the partonic cascades develop in QCD. We will start by analysing the probability that a dipole of mass  $\sqrt{s}$ , i.e. with logarithmic variable  $L = \log(s/s_0)$ , will decay into two dipoles by the emission of a (first) gluon at the value  $\kappa = \log(k_\perp^2/s_0)$ . From the Sudakov factor  $f_{Sud}$  in Eq. (18.49) and the bremsstrahlung cross section we obtain

$$dP = \frac{\alpha_0}{\kappa} d\kappa(L - \kappa) \exp \left[ - \int_\kappa^L \frac{\alpha_0}{\kappa_1} d\kappa_1(L - \kappa_1) \right] \tag{18.59}$$

For the available rapidity range we have introduced the virtual size  $\mu = L - \kappa$  of the dipole at  $\kappa$ . We note that this distribution is not normalised to unity but instead we obtain by integration over  $\kappa$

$$\int_{\kappa_c}^L dP = 1 - f_{Sud}(L, \kappa_c) \tag{18.60}$$

where  $\kappa_c$  is a suitable cutoff. The interpretation is that the probability density  $dP$  is normalised to unity apart from the possibility that the dipole does not decay before we reach  $\kappa_c$ . It is straightforward to perform the integral in the Sudakov factor and, using the variables  $x \equiv \alpha_0\kappa$  and  $y \equiv \alpha_0L$ , we obtain

$$dP = g(y)dx(y - x)x^{y-1} \exp(-x) \tag{18.61}$$

Here  $g(y)$  is a normalisation factor. We may once again use the same methods as we used to find the maximum of the Lund fragmentation distribution in Chapter 9, cf. Eq. (9.6), to prove that there is a pronounced maximum in the distribution for  $x_{max} = y - \sqrt{y}$ ; in terms of  $L, \kappa$  it occurs for  $\kappa_{max} = L - 1/\sqrt{\bar{\alpha}(L)}$ .

There is a simple explanation for this result. The step  $\delta\kappa$  from the starting point  $L$  to  $\kappa_{max}$  is evidently equal to the virtual size of the dipole at  $\kappa_{max}$ . The probability for decay inside this region is then

$$\bar{\alpha}\delta\kappa\delta y = \bar{\alpha}(\delta\kappa)^2 \simeq C \quad (18.62)$$

where  $C$  is a constant of order unity. We will now consider the general case. If a dipole tends to have the same size as its ‘survival time’ this means in the phase-space triangle that a region free of gluons is as wide (in the generalised  $y$ -variable) as it is high (in the  $\kappa$ -direction). This means that *the step  $\delta\kappa$  between two ‘generations’ (meaning the decay-times of the typical dipoles) of gluons behaves as the square root of the virtuality  $\kappa$ .*

Then the first generation (the typical ‘hardest’ single gluon when we start at the virtuality  $L$ ) will occur after a step

$$\delta\kappa_1 \sim C'\sqrt{L}, \quad C' = C/\sqrt{\alpha_0} \quad (18.63)$$

and we are left at the virtuality  $L - C'\sqrt{L}$ . The next generation (containing two ‘typical’ gluons) occurs after a second step

$$C'\sqrt{L - C'\sqrt{L}} \simeq C'\sqrt{L} - (C')^2/2 \quad (18.64)$$

where we have expanded the square root under the assumption that  $C'\sqrt{L} \ll L$ . Counting downwards we obtain after  $n \gg 1$  generations (in which there are  $2^{n-1}$  gluons produced) a remaining virtuality

$$\simeq L - nC'\sqrt{L} + n^2(C')^2/4 \quad (18.65)$$

If this is the endpoint  $\kappa$  we obtain

$$n \simeq 2(\sqrt{\alpha_0 L} - \sqrt{\alpha_0 \kappa})/C \quad (18.66)$$

and the multiplicity of dipoles will be  $2^n$ , so that using  $C = \log 2$  we have

$$M_1 \sim \exp 2(\sqrt{\alpha_0 L} - \sqrt{\alpha_0 \kappa}) \quad (18.67)$$

To obtain  $M_2$  we just multiply by the typical dipole size at  $\kappa$ ; we have thus in a simple way obtained good approximations for  $\langle \lambda \rangle$  and its first  $\kappa$ -derivative, i.e. the average dipole multiplicity.

It is worthwhile to ponder the immensely slow development of a QCD cascade. Suppose that we consider an  $e^+e^-$  annihilation event with  $\sqrt{s} = 1000$  GeV and  $\Lambda_{QCD} = 250$  MeV. Then the first generation will occur, according to the calculation above, at around  $k_\perp \sim 130$  GeV, the second at around  $k_\perp \sim 15$  GeV, the third at around 5 GeV, etc.

Actually we are nevertheless exaggerating the rate. When we take the recoil corrections into account within the so-called modified leading-log scenario the average rate will become even slower.

5 The master equation

In [6] several other distributions are derived and investigated. We will here be satisfied to discuss the combined distribution in the number of dipoles,  $n_d \equiv n$ , and their total length  $\sum_{j=1}^n \mu_j \equiv \lambda$ , which we will call  $P(n, \lambda, \kappa)$  (once again suppressing the dependence on  $L$ ).

The master equation for the distribution  $P(n, \lambda, \kappa)$  is

$$\frac{\partial P}{\partial \kappa} - n \frac{\partial P}{\partial \lambda} = \frac{\alpha_0}{\kappa} \lambda [P(n, \lambda, \kappa) - P(n - 1, \lambda, \kappa)] \tag{18.68}$$

The result stems from the fact that the change in  $\lambda$  from  $n$  independent dipoles is  $\lambda \rightarrow \lambda + n\delta\kappa$  when  $\kappa \rightarrow \kappa - \delta\kappa$ . Further there is a loss for  $P(n)$  and a gain from  $P(n - 1)$  when any of the dipoles decays.

We will briefly consider this equation and its solutions before we show how to incorporate corrections due to recoils, the phase-space size and the neglect of the polarisation sum in the decay process.

We may make Eq. (18.68) into a linear partial differential equation in all the three variables  $n, \lambda, \kappa$  in the approximation when  $n$  is considered a continuous variable. Then Eq. (18.68) becomes

$$\frac{\partial P}{\partial \kappa} - n \frac{\partial P}{\partial \lambda} \simeq \frac{\alpha_0}{\kappa} \lambda \frac{\partial P}{\partial n} \tag{18.69}$$

We may again use the method of rays and look for  $n = n(\kappa)$  and  $\lambda = \lambda(\kappa)$  with the properties that

$$\frac{dn}{d\kappa} = -\frac{\alpha_0}{\kappa} \lambda, \quad \frac{d\lambda}{d\kappa} = -n \tag{18.70}$$

Given the solutions to these equations we then have that

$$\frac{\partial P}{\partial \kappa} + \frac{\partial P}{\partial \mu} \frac{d\lambda}{d\kappa} + \frac{\partial P}{\partial n} \frac{dn}{d\kappa} = \frac{d}{d\kappa} P(n(\kappa), \lambda(\kappa), \kappa) = 0 \tag{18.71}$$

i.e. any function which is constant along the rays will work!

We note that Eqs. (18.70) are just the equations we had for the quantities  $M_j, j = 1, 2$  or  $j = 0, 3$  (Eq. (18.53)) and they can consequently be solved in terms of these functions. We assume that we know the distribution in  $n_0, \lambda_0$ , to be called  $F(n_0, \lambda_0)$ , for a certain value of  $\kappa = l_0$ . It is straightforward to describe the values of  $\lambda, n$  for an arbitrary  $\kappa \leq l_0$  from the results of Eqs. (18.53) with the boundary values  $n_0, \lambda_0$

$$\begin{aligned} n &= n_0 M_1(l_0, \kappa) + \lambda_0 M_0(l_0, \kappa) \\ \lambda &= \lambda_0 M_3(l_0, \kappa) + n_0 M_2(l_0, \kappa) \end{aligned} \tag{18.72}$$

We note in particular that we obtain the correct boundary values  $n = n_0, \lambda = \lambda_0$  when  $\kappa = l_0$  because the functions  $M_1 = M_3 = 1$  and  $M_2 = M_0 = 0$  when the arguments coincide, according to their definitions (Eq. (18.53)). We may then write a simple formula for the total function  $P$  in terms of the boundary-value distribution  $F$ :

$$P(n, \lambda; \kappa) = \int d\lambda_0 dn_0 F(n_0, \lambda_0) \delta(n - n_0 M_1 + \lambda_0 M_0) \delta(\lambda - \lambda_0 M_3 + n_0 M_2). \quad (18.73)$$

The integral is easily solvable, once again using the properties of the functions  $M_j$ :

$$P(n, \lambda, \kappa) = F(nM_3 - \lambda M_0, \lambda M_1 - nM_2) \quad (18.74)$$

It is useful to convince oneself that in this way *the properties of the  $M$ -functions lead to a transfer property for the solutions* (which, of course, is just the content of the original partial differential equation). By this we mean that if the distribution  $F$  at  $l_0$  is described in terms of the distribution  $G$  at another  $\kappa = l_1 \geq l_0$  then the formulas are identical if we exchange  $F$  for  $G$  and the argument  $l_0$  for  $l_1$ . The changes in the system are all the time evidently occurring in the average way, according to the relevant average values of  $\lambda$  and  $n$ , as we can see from Eqs. (18.53) and (18.70).

The conclusion is that in this approximation the ensemble of states described by  $F$  at  $\kappa = l_0$  will move on towards different  $(n, \lambda)$ -values at other  $\kappa$ -values *but a constant distribution occurs along the rays described by Eq. (18.72)*. The system corresponds to a hamiltonian flow in a space where the coordinate corresponds to  $\lambda$  and the momentum corresponds to the dipole multiplicity  $n$  and the hamiltonian is

$$H = +\frac{n^2}{2} - \frac{\bar{\alpha}\lambda^2}{2} \quad (18.75)$$

At first sight the function  $P$  would seem to provide a possible tool to investigate the running of the QCD coupling constant. Thus it is possible to concentrate on an event sample in which each event contains a number of jets (related to  $n$ ), the combined logarithmic phase space (related to  $\lambda$ ) having a certain cut in the transverse jet energies (related to  $\kappa$ ). Then one would continue with the same event sample using smaller transverse jet energy cuts and study the changes in the distribution in the number of jets and phase-space size. To perform a reliable such comparison it is, however, necessary to make a better approximation than  $P(n) - P(n-1) = \partial P / \partial n$  and also to correct for recoils along the cascade.

In order to investigate the difference between a continuous and a discrete treatment of the multiplicity we will briefly consider a simplified model.

Suppose that we consider e.g. a population of bacteria and assume that as time  $t$  passes the population increases at a constant rate  $\gamma$ . This leads to the following differential equation for the bacteria multiplicity  $P(n, t)$ :

$$\frac{dP}{dt}(n, t) = \gamma[P(n-1, t) - P(n, t)] \quad (18.76)$$

i.e. there is a gain per time unit  $\gamma$  from  $n-1$  and a corresponding loss to  $n+1$ . Using the generating function  $\mathcal{P}(z, t) = \sum P(n, t)z^n$  we obtain the differential equation

$$\frac{d\mathcal{P}}{dt} = \gamma(z-1)\mathcal{P} \quad (18.77)$$

with the obvious solution  $\mathcal{P} = z \exp[\gamma(z-1)t]$  if we start with a single bacterium at  $t=0$ . Expanding the generating function we obtain as expected a Poissonian distribution (truncated at  $n=1$ ):

$$P(n, t) = \frac{(\gamma t)^{n-1}}{(n-1)!} \exp(-\gamma t), \quad n \geq 1 \quad (18.78)$$

If we use the continuous approximation, i.e. put  $P(n) - P(n-1) = \partial P / \partial n$ , we obtain by the method of rays that  $n(t) = \gamma t + 1$ , which obviously corresponds to the mean value of the distribution in Eq. (18.78). Although the mean value is the only size parameter in a Poissonian distribution it is obviously not a good approximation to write the distribution in Eq. (18.78) as a  $\delta$ -distribution and neglect the width. It is, however, possible to include the width if we also take the second derivative into account. In this simple model we obtain

$$\frac{\partial \mathcal{P}}{\partial t} + \gamma \frac{\partial \mathcal{P}}{\partial n} = \frac{\gamma}{2} \frac{\partial^2 \mathcal{P}}{\partial n^2} \quad (18.79)$$

This corresponds to a diffusion equation and we are then very close to the considerations in Chapter 10 on the Brownian motion in impact space in multiperipheral ladder diagrams and in Chapter 12 on the transverse momentum generation. We obtain immediately the well-known (normalised) gaussian solution,

$$\frac{1}{\sqrt{2\pi\gamma t}} \exp\left[-\frac{(n-1-\gamma t)^2}{2\gamma t}\right] \quad (18.80)$$

and this coincides (as it should of course) with a stationary-phase approximation to the Poissonian distribution in Eq. (18.78). It is useful to carry through the calculations, using the Stirling approximation to the factorial.

We conclude that the QCD cascade evolutions do not only correspond to simple 'laminar flow along the mean streamlines', which is what Eq. (18.73) implies, if we use a hydrodynamical analogy. There is also diffusion among the streamlines because of the discreteness in the dipole multiplicity. When

we take the second derivative into account we obtain what is known as the Fokker-Planck equations and there is a very general mathematical method to treat equations of this kind. We have already discussed the Langevin equation in Chapter 12 and we may apply it again, this time coupled to the ray equations which we obtained in the approximate treatment in connection with Eq. (18.69). If we again introduce a gaussian noise term  $R$  with properties in accordance with Eq. (12.19) we may write the following system of coupled stochastic equations:

$$\begin{aligned}\frac{d\lambda}{d\kappa} &= -n \\ \frac{dn}{d\kappa} &= -\bar{\alpha}\lambda + R\sqrt{\bar{\alpha}\lambda/2}\end{aligned}\quad (18.81)$$

The square root in front of the gaussian noise term is this time not a constant but it is nevertheless possible to prove that the resulting equations actually converge to the solution of the equation

$$\frac{\partial P}{\partial \kappa} - n \frac{\partial P}{\partial \lambda} = \frac{\alpha_0}{\kappa} \lambda \left( \frac{\partial P}{\partial n} - \frac{1}{2} \frac{\partial^2 P}{\partial \kappa^2} \right) \quad (18.82)$$

(note that the variable  $\kappa$  decreases!). We will, however, end the investigation at this point.

#### 18.4 The next-to-leading-order corrections

In order to obtain a better approximation it is not only necessary to go back to the discrete  $n$ -distribution, but it is also necessary to improve upon the master equation. We note in particular that we have up to now considered the phase space to be given by the triangular approximation

$$|y| \leq \log(\sqrt{s}/k_{\perp}) \quad \text{instead of} \quad k_{\perp} \cosh y \leq \frac{\sqrt{s}}{2} \quad (18.83)$$

which would e.g. imply that the maximum  $k_{\perp max}^2 = s/4$  instead of  $s$ . We have also neglected the polarisation sums in the cross section, i.e. that the emission of a  $g$  from a  $q\bar{q}$  should be weighted with the factor  $x_1^2 + x_3^2$ . This is again a factor which starts to play a role close to the triangle boundary, because at the boundary either  $x_1$  or  $x_3$  is small. The polarisation sum has all the time been approximated by 2 and to check on the approximation we will consider the integral

$$I \equiv \int_{y_{min}}^{y_{max}} dy (x_1^2 + x_3^2) \quad (18.84)$$

for a fixed value of  $k_{\perp}$ . According to our approximation  $I = 2\log(s/k_{\perp}^2)$  but if we introduce (cf. the definitions in Eq. (16.39))

$$x_1 = 1 - k_{\perp} \exp(-y)/\sqrt{s}, \quad x_3 = 1 - k_{\perp} \exp y/\sqrt{s} \quad (18.85)$$

then we obtain a correction term, i.e.

$$I = 2[\log(s/k_{\perp}^2) - \delta_q] \quad (18.86)$$

$$\delta_q = \frac{3}{2} \sqrt{1 - \frac{4k_{\perp}^2}{s}} - 2 \log \left[ \frac{1}{2} \left( 1 + \sqrt{1 - \frac{4k_{\perp}^2}{s}} \right) \right]$$

It turns out that the correction term varies very little as a function of  $k_{\perp}$  and that if we cut off a strip  $c_q/2 = 3/4$  on each side of the triangle we obtain a very good approximation to the suppression from the polarisation sum as well as to the neglected hyperbolic cutoff, Eq. (18.83).

It is possible [72] to subdivide the phase space for gluon emission into regions relevant to  $q\bar{q}$ -,  $qg$ -,  $g\bar{q}$ - and  $gg$ -dipoles. They all have different polarisation sums according to the dipole cascade model, Eq. (17.2), and for all of them one can calculate the decrease in the triangles. The corresponding decrease factor for gluon corners is e.g.  $c_g = 11/6$ . It is also possible to include gluon splitting as implemented in the dipole cascade model [10] and finally also to take into account the effective coupling constants,  $3\alpha_s/2\pi$  and  $4\alpha_s/3\pi$ , respectively.

The result is a rather complex set of equations, [72], which are close to the so-called modified leading-log approximation in QCD, [52]. Using the correction terms in the  $L$ -method the result becomes a very good approximation to the Monte Carlo results for the multiplicity moments.

We will not go into the details but will briefly consider the simplest and actually also the largest correction to the master equation, Eq. (18.68). If we decrease all the  $n$  dipoles by a common factor  $c$  then we obtain

$$\frac{\partial P}{\partial \kappa} - n \frac{\partial P}{\partial \mu} = \frac{\alpha_0}{\kappa} \{(\lambda - nc)P(n, \lambda, \kappa) - [\lambda - (n - 1)c]P(n - 1, \kappa, \lambda)\}. \quad (18.87)$$

From this equation we can easily calculate the equations connecting the (modified) mean multiplicity  $M_{m1}$  and mean  $\lambda$ -phase space size,  $M_{m2}$ . We obtain

$$\frac{dM_{m1}}{d\kappa} = -\frac{\alpha_0}{\kappa}(M_{m2} - cM_{m1}), \quad \frac{dM_{m2}}{d\kappa} = -M_{m1} \quad (18.88)$$

which should be compared with Eqs. (18.53). There is then a second-order differential equation for  $M_{m2}$ :

$$\frac{d^2 M_{m2}}{d\kappa^2} = c \frac{\alpha_0}{\kappa} \frac{dM_{m2}}{d\kappa} + \frac{\alpha_0}{\kappa} M_{m2} \quad (18.89)$$

This equation again has solutions in terms of the modified Bessel functions. We may define the functions

$$\begin{aligned}\mathcal{I}_\beta(\kappa) &= \sqrt{2}\kappa^{\beta/2}I_\beta(2\sqrt{\alpha_0\kappa}) \\ \frac{d\mathcal{I}_\beta}{d\kappa} &\equiv \mathcal{I}_{\beta-1} = \sqrt{2\alpha_0}\kappa^{(\beta-1)/2}I_{\beta-1}(2\sqrt{\alpha_0\kappa})\end{aligned}\quad (18.90)$$

for  $\beta = 1 + \alpha_0 c$  (we note the similarities to the functions  $\mathcal{I}_j$ ,  $j = 0, 1$ , in Eqs. (18.21)) and similarly the functions  $\mathcal{K}_\beta$  with respect to the modified Bessel functions  $K$ , with a minus sign in the derivative. Then the solution for  $M_2$  is

$$\begin{aligned}M_{m2} &= L^{1-\beta}[\mathcal{I}_\beta(L)\mathcal{K}_\beta(\kappa) - \mathcal{I}_\beta(\kappa)\mathcal{K}_\beta(L)] \\ M_{m1} &= L^{1-\beta}[\mathcal{I}_\beta(L)\mathcal{K}_{\beta-1}(\kappa) + \mathcal{I}_{\beta-1}(\kappa)\mathcal{K}_\beta(L)]\end{aligned}\quad (18.91)$$

if we start at  $\kappa = L$  with  $M_{m2} = 0$  and  $M_{m1} = 1$ . The asymptotic behaviour for  $L \gg \kappa \gg 0$  is

$$M_{m2} \sim \left(\frac{L}{\kappa}\right)^{-\alpha_0 c/2} (L\kappa)^{1/4} \exp[2(\sqrt{\alpha_0 L} - \sqrt{\alpha_0 \kappa})] \quad (18.92)$$

Evidently the introduction of a factor that diminishes the phase space is reflected directly in the power in front of the exponents, which has changed from  $1/4$  to  $1/4 - \alpha_0 c/2$  as compared to Eqs. (18.17) and (18.24). This factor directly reduces the  $L$ -dependence and increases the  $\kappa$ -dependence. The result is an even slower development of the cascades than in the LLA, described earlier.

### 18.5 On the running coupling in QCD

The equations for the  $\lambda$ - and  $n$ - variations with  $\kappa$  have a great similarity to the Callan-Symanzik equations, considered in Chapter 4. The background is, however, completely different. Equations (18.68) and (18.87) are derived from classical probability concepts. They are really classical gain-loss equations and there is not the renormalisation group background which may motivate a relationship to a Callan-Symanzik investigation. We have changed the scale from  $\kappa$  to  $\kappa - d\kappa$  and then there is in this step a possibility that the number of dipoles  $n$  increases to  $n + 1$ , which for the equations mentioned above corresponds to a loss. But there is also a gain if the state changes from  $n - 1$  to  $n$ .

The probability is governed by the relevant coupling, which mostly corresponds to the situation in gluon dipoles and therefore equals  $3\alpha_s/2\pi$ . This effective coupling is multiplied by the available phase space  $\lambda$  and the probability of finding just this number of dipoles at  $\lambda$ . The running of

the coupling is introduced by hand, i.e. we use

$$\alpha_s = \left( \frac{12\pi}{33 - 2n_f} \right) \frac{1}{\kappa} \tag{18.93}$$

Now suppose that (without any further motivation) we introduce the running of the coupling in our equations along the same lines as in the Callan-Symanzik equations. That would mean that we would have an accompanying scale change of  $\partial/\partial\kappa$  to  $\partial/\partial\kappa + \beta\partial/\partial\alpha_s$  in the equations (at the same time, of course, we leave out the running of  $\alpha_s$  in Eq. (18.93) and introduce this property through the  $\beta$ -dependence).

This means in the language of gain-loss equations that we introduce a loss term which looks like

$$\begin{aligned} -\beta(\alpha_s) \frac{\partial \mathcal{P}}{\partial \alpha_s} &= \left( \frac{11}{6} \frac{3\alpha_s}{2\pi} - \frac{2}{3} \frac{n_f \alpha_s}{4\pi} \right) \alpha_s \frac{\partial \mathcal{P}}{\partial \alpha_s} \\ &\equiv (\delta y_g \alpha_{effg} - \delta y_q \alpha_{effq}) \mathcal{N}(\mathcal{P}) \end{aligned} \tag{18.94}$$

The results in the first line correspond to straightforward algebra, using the expressions for the  $\beta$ -function and the running coupling constant of QCD. The symbol  $\mathcal{N}(\mathcal{P})$  indicates a number operator in the sense that for any well-behaved function  $f = f(\alpha)$  we obtain an average  $n$  with

$$f = \sum \alpha^n a_n, \quad \alpha \frac{\partial f}{\partial \alpha_s} = \sum n \alpha^n a_n \equiv \mathcal{N}(f) \tag{18.95}$$

The two effective couplings

$$\alpha_{effg} = \frac{3\alpha_s}{2\pi}, \quad \alpha_{effq} = \frac{n_f \alpha_s}{4\pi} \tag{18.96}$$

correspond to the gluon emission process  $g \rightarrow gg$  and the gluon splitting process  $g \rightarrow q\bar{q}$ , respectively. Finally the two quantities  $\delta y$  are, respectively,

$$\begin{aligned} \delta y_g &= \frac{11}{6} \rightarrow 2 \log(s/k_\perp^2) - \int_{y_{min}}^{y_{max}} dy (x_1^3 + x_3^3) \\ \delta y_q &= \frac{2}{3} = \int_0^1 dz [z^2 + (1-z)^2] \end{aligned} \tag{18.97}$$

We met the quantity  $\delta y_g$  above as the decrease in phase space for emission of new gluons in the neighborhood of a gluon corner. It can most reasonably be considered as a *typical collinearity size in rapidity* for a fixed value of  $k_\perp$  in the limit when  $s \rightarrow \infty$ .

The quantity  $\delta y_q$ , however, is for a fixed  $k_\perp$  and the same limit in  $s$  the total rapidity phase space for a gluon to split into a  $q\bar{q}$ -pair.

Therefore such a variation added to the coupling constant in the master equation, and for that matter to any of the partial differential equations used in the  $\kappa$ -method, may be considered as

- a loss term proportional to the probability that the gluon fluctuates into a  $gg$ -pair within a small collinearity region. Intuitively that region should be equal to the region in phase space where such virtual fluctuations may occur in this approximation;
- a gain term proportional to the probability that the gluon may fluctuate into a  $q\bar{q}$ -pair. The rapidity size allowed for such a fluctuation is essentially smaller because there is no pole in  $z$ , which means that it exponentially falls off in rapidity from the gluon corner.

This interpretation of the running coupling constant is certainly somewhat imaginative, in particular the interpretation that the collinearity region is equal to the region of virtual fluctuations for the gluon.

We nevertheless note that if a gluon fluctuates into a  $gg$ -pair then there is a color flow across the region. But if it fluctuates into a  $q\bar{q}$ -pair then the color flow is broken over the corresponding region. Thus a gluon is never in the first case able to get away from the influence of its own Coulomb color field, but in the second case there is nothing to stop it moving around as a free asymptotic pair.

Another way to understand the gain-loss nature of the gluon emission and gluon splitting, respectively, is to consider the case when a gluon just above  $\kappa$  decays into two gluons (which then are counted at  $\kappa$ ). Just below  $\kappa$ , however, the two gluons are reabsorbed into a single gluon again, thereby causing a loss in multiplicity. But if the gluon instead splits into a  $q\bar{q}$ -pair there is no gluon at  $\kappa$ , but if the pair reassembles to a gluon there will then be a gain in the gluon multiplicity. Note that the possibility of a loss term only occurs in a nonabelian gauge theory, because the abelian photons do not interact.

## 18.6 Discrete QCD, another approximation method

### 1 The method

We will in this section make explicit use of the properties of the running coupling, discussed in section 18.5, to present another analytical approximation method for the perturbative QCD parton cascades. It is called *discrete QCD*, [15], for reasons easily understood when it is demonstrated. To that end we start by using the Webber-Marchesini method to search through the triangular phase space, cf. Section 17.7.

This means that we will take steps in the rapidity  $y$  and consider the probability of obtaining a gluon emission in each step. We will in particular choose to make these steps *finite* in size, and equal to  $\delta$ . Consider as an illustration the rapidity bin  $\delta y_1 \equiv \delta$  around  $y_1$  in Fig. 18.1 and assume

that there is one emission for  $\kappa$  and none between  $\kappa$  and the maximum  $\kappa_{max} \equiv \ell_1$  in this bin. The resulting probability is given by (note, see subsection 3 of section 17.3, the Sudakov factor!)

$$dP(\kappa, \ell_1) = \frac{(\alpha_0 \delta) d\kappa}{\kappa} \exp(-\alpha_0 \delta) \int_{\kappa}^{\ell_1} \frac{d\kappa'}{\kappa'} = d\kappa (d\kappa^{d-1} \ell_1^{-d}) \quad (18.98)$$

with  $d = \alpha_0 \delta$ . As yet we have not decided upon the size of  $\delta$  but it is perfectly feasible to choose

$$\delta = \frac{1}{\alpha_0} \simeq \delta y_g = \frac{11}{6} \quad (18.99)$$

Here we have made the approximation of neglecting the contribution from the gluon splitting into  $q\bar{q}$ -pairs, or equivalently we have put the number of flavors  $n_f = 0$  in the running coupling, cf. Eq. (18.97). In this way the power  $d$  in Eq. (18.98) becomes 1 and we obtain the simple result that *there is no  $\kappa$ -dependence left* in the probability

$$dP(\kappa, \ell_1) = \frac{d\kappa}{\ell_1} \quad (18.100)$$

This evidently goes for all steps of size  $\delta \simeq \delta y_g$  and in particular for a (discrete) value of  $L = \log(s/s_0) = 2N\delta$  the whole ‘original’ dipole phase-space triangle will contain  $2N$  possible emissions.

We now make the further assumption that inside each  $\delta$ -bin in rapidity the  $\kappa$ -variable is discretised so that  $\ell_1 = n_1(2\delta)$  with  $n_1$  an integer (the index 1 means the bin with the height  $\ell_1$ ). The result is that there may be any  $n$ -emission,  $1 \leq n \leq n_1$ , i.e. an emission in the  $\kappa$ -box  $n$ , with the same probability  $P_n(n_1)$  for all integer  $n$ , where

$$P_n(n_1) = \frac{1}{n_1} \quad (18.101)$$

Each emission will produce a subtriangle, cf. section 17.5, which again contains  $2n$  discrete steps in rapidity along the projecting folds. This means  $n$  steps on each of the two sides, see Fig. 18.1. The whole procedure can evidently be continued with new discretised (sub-)triangular folds, projecting folds, and so on. It is easy to convince oneself that (apart from the very outskirts of the phase-space triangles) the construction is consistent and that the above-mentioned  $\kappa$ -boxes fit in. Note that it is necessary to take  $2\delta$ -steps in  $\kappa$  for this consistency!

So what is the physics behind this seemingly simple but up to now purely mathematical scheme? We are actually doing exactly what the running coupling in QCD indicates to us, i.e. we are sending out the gluons with a distance at least  $\delta y_g = 11/6$  between them. If they are closer than this distance in rapidity then they will in practice be reabsorbed, i.e. with this

method we emit *effective gluons*, which are not reabsorbed in the next step in perturbation theory!

This is also an instructive example of the difference between *exclusive distributions*, with a probability normalised to one event having certain properties and *inclusive distributions*, which instead correspond to the average behaviour of many events. Therefore the results should in the latter case rather be called densities. The running coupling is characteristic for the inclusive density of gluons, but if we concentrate on the largest gluon then the probability is the same constant for all emissions!

There are two regions which need particular attention. The first is the region corresponding to  $n = 1$ , i.e. the lowest  $\kappa$ -box in each  $\delta y_g$ -step. We will interpret this box to correspond to no emission, i.e. the effective gluons in such a box are too soft to be noticeable. This means that we are actually bringing in a precise cutoff in the cascades with respect to  $\kappa$ , i.e. all ‘observable’ gluons have  $\kappa \geq 2\delta y_g$ .

The second comprises the regions close to the triangular border in each phase-space triangle, where the boxes are distorted. We have actually already discussed these regions repeatedly because the triangular border corresponds to gluons collinear with the parton emitting them. Just as in connection with the modified leading-log approximation, e.g. in Eq. (18.87), we will cut away a region equal to  $\delta y_g/2$  along each border of the triangles. (We note that we are in this way making a small error for dipoles containing a  $q$ - or  $\bar{q}$ -particle as endpoint. For this case we should cut away the slice  $\delta y_q/2 = 3/4$ , which is less than the value of  $\delta y_g/2$  according to Eq. (18.86)).

## 2 Some results in discrete QCD

We will now consider in some detail the structure of the scheme developed in the last subsection. The original dipole triangle will be called an *N-forest* (actually containing  $2N$  bins) because in each  $\delta y_g$  rapidity bin in the original dipole there will be a tree-like structure, which we will call an  $n_1$ -tree (with the maximum  $\kappa$  in the bin equal to  $n_1 2\delta y_g$ ).

Such an  $n_1$ -tree will, however, not necessarily have height  $n_1$ . But it will have two sides, each with length  $n\delta y_g$  if there is an emission at  $\kappa = n2\delta y_g$  (with  $n \leq n_1$ ). This is illustrated in Fig. 18.5, which corresponds to the triangular phase space with its projecting folds looked upon from below.

The two sides of the tree correspond to the two sides of the projecting emission triangle according to the construction in subsection 17.5 (remember that each fold has length  $n\delta y_g$ ). We will call this a *true n-tree*. We note that in this way the  $n_1$ -tree is a true  $n$ -tree, with each  $n$  occurring, according to Eq. (18.101), with the same probability, i.e.  $1/n_1$ .

It is worthwhile noting the following two features.

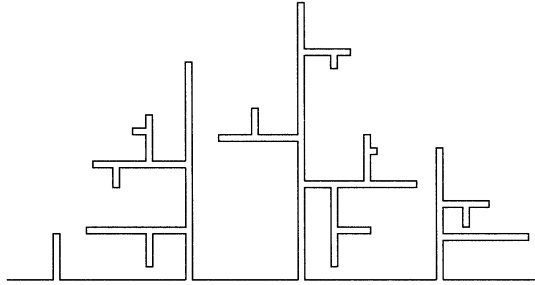


Fig. 18.5. The projecting folds of the phase-space triangle together with a set of subfolds and subsubfolds, etc.

- The two sides of the true tree correspond to the two color flows at a gluon corner. A gluon with e.g. the color combination  $r\bar{g}$  contains one  $r$ -color flowing towards the gluon tip and one  $g$ -color starting at the gluon tip and flowing ‘inwards’ (being an anticolor its flow is oppositely directed to the color). The connection point between them is the ‘top’ of the true tree and they are each color-connected to partons on both sides of the emitted gluon.

It may seem for the projecting triangular fold in e.g. Fig. 18.1 that the two parts of the folds adjacent to the original background triangle are close in the rapidity variable of this original dipole. This is not true; they are actually far apart in true rapidity and in particular also distant with respect to color flow. The distance in true rapidity is just the distance from the bottom of the true  $n$ -tree up to the top and down again i.e.  $n2\delta y_g$ .

- A true  $n$ -tree actually has the same structure as an  $n$ -forest defined above (to see this cut it up along the centre line, i.e. along the gluon corner, see Fig. 18.5). Therefore all statements for one can be taken over to the other.

Each side of a true  $n$ -tree is now subdivided into  $n$  bins, containing ‘ $n'$ -trees’ (in realistic tree-language it may possibly be better to refer to them as branches) with  $n' = 1, \dots, n$ . Each such tree can be treated just as the first one, i.e. it will contain a true tree with two sides each of a length at most equal to the length of the original tree. Further, all integer values have the same probability according to Eq. (18.101). Everything ends at the place where the probability is just 1 of obtaining a 1-tree everywhere, i.e. the situation which we have defined above to correspond to no further gluons.

As an example of what we can easily obtain consider the probability that an  $n$ -tree contains exactly  $m$  gluons,  $P(m; n)$ . We will also introduce the probability distribution,  $P^t(m; n)$ , that a true  $n$ -tree contains exactly  $m$  gluons and finally we define the corresponding generating functions,  $\mathcal{P}(z; n)$  and  $\mathcal{P}^t(z; n)$ , with e.g.

$$\mathcal{P}(z; n) = \sum z^m P(m; n) \tag{18.102}$$

Then there are two easily understood properties.

- 1 An  $(n + 1)$ -tree is either a true  $(n + 1)$ -tree with probability  $x_{n+1} = 1/(n+1)$  or else an  $n$ -tree with probability  $y_{n+1} = 1 - x_{n+1} = n/(n+1)$ , i.e.

$$\begin{aligned} \mathcal{P}^t(z; n + 1) &= \frac{\mathcal{P}(z; n + 1) - y_{n+1}\mathcal{P}(z; n)}{x_{n+1}} \\ &= (n + 1)\mathcal{P}(z; n + 1) - n\mathcal{P}(z; n) \end{aligned} \tag{18.103}$$

- 2 The difference between a true  $(n + 1)$ -tree and a true  $n$ -tree is that one gets in the first case contributions also from the two largest subtrees, i.e. one  $n$ -tree on each side:

$$P^t(m; n + 1) = \sum_{\sum m_j = m} P(m_1; n)P^t(m_2; n)P(m_3; n) \tag{18.104}$$

or equivalently in terms of the generating functions

$$\mathcal{P}^t(z; n + 1) = [\mathcal{P}(z; n)]^2 \mathcal{P}^t(z; n) \tag{18.105}$$

It is as always necessary to supply the boundary conditions and in this case we obtain easily  $\mathcal{P}^t(z; 1) \equiv \mathcal{P}(z; 1) = 1$  and  $\mathcal{P}(z; 2) = (1 + z)/2$ . It is then straightforward to construct all the distributions.

Actually the formulas we have derived are discretised versions of the  $L$ -method formulas described in subsection 1 (although we have written them for the multiplicities and not for the  $\lambda$ -measure as there). This is shown in [15] and in this reference there are also a number of other applications mentioned, i.e. the  $\lambda$ -measure distributions, the combined distributions of the  $\lambda$ -measure and the multiplicities, how to go to the formulas of the  $\kappa$ -method and finally also a way to translate the results from this lattice description in an abstract space to the observable energy-momentum vectors of the emitted gluons.

As an example we consider the average multiplicity for an  $N$ -tree,  $\bar{n}(N)$ . This can as usual be obtained from the generating function,  $\mathcal{P}(z; N)$ , by means of the first derivative evaluated for  $z = 1$ ; note that  $\mathcal{P}(z = 1; n) = \mathcal{P}^t(z = 1; n) = 1$  always. We obtain from Eqs. (18.103) and (18.105) after

some small manipulations:

$$\bar{n}(N+1) - 2\bar{n}(N) + \bar{n}(N-1) = \frac{2}{N+1}\bar{n}(N-1) \quad (18.106)$$

which as expected is a discretised version of e.g. Eqs. (18.54) and (18.89). The result is a very good description of the jet multiplicities as obtained from Monte Carlo simulations by ARIADNE, see [15].

We end with a few remarks on the results of discrete QCD:

- Despite the discretisation approximation the resulting formulas for the jet multiplicities and hadron multiplicities are even better approximations to the Monte Carlo simulation results (including all the kinematics) than any modified leading-log result.

This may seem surprising but it is related to the fact that the ‘reabsorption’ length in rapidity we have introduced, i.e.  $\delta y_g$ , is also a good description of the rapidity region where the recoils from earlier emissions are noticeable.

- It turns out that if we consider the zeroes of the generating function, i.e. the values  $z_j(n)$  with

$$\mathcal{P}(z; n) = A_n \prod [z - z_j(n)] \quad (18.107)$$

where  $A_n$  is a suitable constant, then these quantities exhibit some surprising properties. They are all finite and stay in a region close to the origin in a structure called a Julia set by the mathematicians. Its properties are just as beautiful as those of the nowadays well-known Mandelbaum set. Each root of the generating function will according to Eq. (18.105) change into three when  $n \rightarrow n+1$  and they are also closely located, albeit occurring in an irregular fashion nowadays known as a fractal curve.

Instead of going into the details (which are still under investigation) we will exhibit these irregularities in a different way in the next section.

It is finally of some interest to connect the formulas obtained in the discrete QCD model to the ordering procedure used in the dipole cascade model, i.e. to investigate how the particular basic property of discrete QCD, occurring in Eqs. (18.98) to (18.101), will come out of our ordinary treatment of the Sudakov factor. Then we return to Eq. (18.59) (cf. also Eq. (18.49)), which describes the first decay of a dipole with logarithmic squared mass  $L$  into two dipoles by a gluon emission at  $\kappa_1$ :

$$dP_1 = \frac{\alpha_0}{\kappa_1} d\kappa_1 (L - \kappa_1) f_{Sud}(L, \kappa_1) \quad (18.108)$$

This formula is valid in the leading-log approximation and it is easy to extend it to the modified leading-log approximation by the exchange  $L \rightarrow L - 1/\alpha_0$  (assuming that we neglect the flavored dipoles). This means that the rapidity space factor is changed from  $L - \kappa_1$  to  $L - \kappa_1 - 1/\alpha_0$  and the Sudakov factor will change to  $f_{Sud}(L - 1/\alpha_0, \kappa_1)$ . We now introduce the variables  $2\ell \equiv \alpha_0 L$  and  $2k_1 \equiv \alpha_0 \kappa_1$  and perform the Sudakov integral, to obtain in the modified leading-log approximation

$$f_{Sud}(L - 1/\alpha_0, \kappa_1) \simeq \frac{k_1^{2\ell - 2k_1} \Gamma^2(k_1)}{\Gamma^2(\ell)} \quad (18.109)$$

$$dP_1 = dk_1 [2(\ell - k_1) - 1] \frac{k_1^{2\ell - 2k_1 - 1} \Gamma^2(k_1)}{\Gamma(\ell)^2}$$

We have used the Stirling approximation for the  $\Gamma$ -functions:

$$\Gamma(\ell) \simeq C \exp[(\ell - 1/2) \log \ell - \ell] \quad (18.110)$$

with  $C$  a normalisation constant.

In order to understand the result we return to the distributions of discrete QCD and interpret  $\ell, k_1$  as integers.

Consider the probability of emitting no gluon in an  $\ell$ -forest with a ‘tree-height’ above  $k_1$ . Then for a  $j$ -tree with  $j \leq k_1$  the probability is obviously 1 because there can be no true  $k_1$ -tree in this case. For a  $(k_1 + m)$ -tree, when the probability is  $1/(k_1 + m)$  for each integer ‘height’, there are  $m$  possibilities for making a true tree above  $k_1$  and thus the probability of using none of them is  $1 - m/(k_1 + m) = k_1/(k_1 + m)$ .

The probability  $dP_1/dk$  in Eq. (18.109) contains two factors. The first corresponds to the number of ways that one can choose any one of the ‘central’ integer  $y$ -bins of height  $k_1 + 1, \dots, \ell - 1, \ell - 1, \dots, k_1 + 1$ . The second is the probability of making an effective gluon at  $k_1$  in one of these bins and only gluons below  $k_1$  in the rest of the bins.

The observant reader will note that there seems to be a mismatch, i.e. there is a factor  $2(\ell - k_1) - 1$  for the number of bins but only  $2(\ell - k_1) - 2$  central integers. A closer examination tells us, however, that the two  $k_1$ -bins, one on each side, should be incorporated in the possibility of making a true  $k_1$ -tree. Due to the triangular shape, however, the surface related to them is only half the surface related to those called central. Therefore the problem is solved if we incorporate them with unit probability and phase space size  $1/2$  each.

Next we consider a second gluon emission at  $\kappa_2 < \kappa_1 < L$ . It is straightforward to prove (and the reader is strongly invited to think it through, in particular the factorisation property of the Sudakov factors!) that with proper Sudakov factors this probability is, in the modified

leading-log approximation,

$$dP_2 = (\kappa_0 - \kappa_1 - 1/\alpha_0)(\kappa_0 + \kappa_1 - 2\kappa_2 - 2/\alpha_0) \\ \times \prod_{j=1}^2 d\kappa_j \frac{\alpha_0}{\kappa_j} f_{Sud}(\kappa_{j-1} - 1/\alpha_0, \kappa_2) \quad (18.111)$$

where we have introduced the symmetric notation  $L \equiv \kappa_0$ . The two factors in front of the product sign correspond to the size of the original dipole when it decays at  $\kappa_1$  and the sum of the sizes of the two emerging dipoles at  $\kappa_2$ . We again leave it to the reader to prove in terms of the  $k_j = \alpha_0 \kappa_j / 2$  variables that Eq. (18.111) can be written as

$$dP_2 = (2k_0 - 2k_1 - 1)dk_1(2k_0 + 2k_1 - 2k_2 - 2)dk_2 \\ \times \prod_{j=0}^1 \frac{\Gamma^2(k_2)k_2^{2k_j-2k_2}}{\Gamma^2(k_j)} \prod_{j=1}^2 \frac{1}{k_j} \quad (18.112)$$

and from this result it is obvious how to generalise the formulas to any number of gluon emissions. In terms of the notions of discrete QCD we conclude that if  $n$  gluon folds are produced at the integers  $k_1, \dots, k_n$  in an original  $k_0$ -forest then we have the following.

- For the emission of a gluon at  $\kappa_j \equiv 2k_j/\alpha_0$  one should multiply by the number of possibilities for choosing a (generalised) rapidity bin (including the outer two with a common size 1). This is equal to the sum of all the virtual dipole sizes, i.e. to the size of the  $\lambda$ -measure at the virtuality  $\kappa_j$ , including the modified leading-log correction. For the case  $n = 2$  this corresponds to the first two terms in Eq. (18.112).
- For the triangles that correspond to such a gluon emission one should multiply by the probability of making no true tree above  $k_n$ . This is the first product in Eq. (18.112)
- The running coupling, which in this notation corresponds to the last product term, then contains the probability of making a true  $k_j$ -tree in the central bin of each triangular fold, i.e. of the gluon being produced at  $\kappa_j = 2k_j/\alpha_0$  (note that there is no  $1/k_0$ -factor and also note that the last factor  $1/k_n$  can be interpreted as discussed in connection with the first gluon emission in Eq. (18.109). The emitted gluons can evidently be attached at any integer value along the relevant  $\lambda$ -size.

If this result is integrated over all the  $\kappa_j$ -variables we actually obtain a general formula for the distribution  $P(\lambda, n, \kappa)$ . It is a solution to the differential equation in Eq. (18.87) (with the parameter  $c = 1/\alpha_0$ ), as the reader can readily verify by iteration from  $n = 1$  upwards.

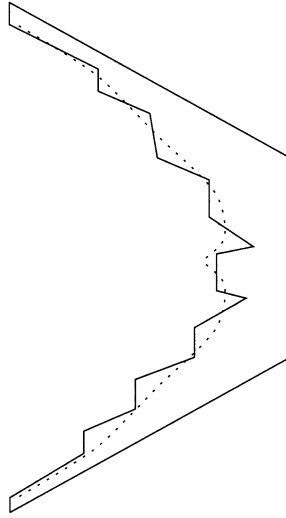


Fig. 18.6. The particles produced in connection with the fragmentation in Fig. 15.17 are redrawn along the directrix, together with the two connected hyperbolas (dotted).

## 18.7 The $x$ -curve and an infrared-stable $\lambda$ -measure

### 1 Definitions

An undesirable feature in the present definition of the generalised rapidity space region  $\lambda$  is that it can only be defined as long as the dipole (squared) masses are above a certain value  $s_0$ . We will in this section introduce an infrared-stable definition of  $\lambda$  and also a well-defined curve, [20], the  $x$ -curve, which describes the average energy-momentum-space behaviour of the final-state particles.

In order to understand the idea behind the  $x$ -curve consider Fig. 18.6. In this picture the yoyo-hadrons, which are produced around the two hyperbolas in Fig. 15.12, are drawn instead as a series of connected line-segments close to the two hyperbolas spanned along the directrix. They are of course the same hadrons but while their production points are emphasised in Fig. 15.17 it is instead their energy-momentum vectors which play the role of connectors in Fig. 18.6. The curve exhibited in this way is (approximately) the  $x$ -curve.

For a mathematical description we define a function  $T(\xi) \equiv \exp[\lambda(\xi)]$  and a vector  $q(\xi)$  along the directrix  $A(\xi)$  by means of differential equa-

tions (we imagine that the directrix is parametrised by the parameter  $\xi$  and that it is differentiable so that  $dA$  has a meaning as a four-vector):

$$dT = \frac{(qdA)T}{m_0^2}, \quad dq = dA - \frac{(qdA)}{m_0^2}q \tag{18.113}$$

For the vector  $q$  we obtain formally, with boundary value  $q(\xi = 0) = 0$ , that it is a weighted mean of the partonic energy-momentum vectors which describe the directrix according to e.g. subsection 17.6:

$$q(\xi) = \frac{1}{T(\xi)} \int_0^\xi dA(\xi')T(\xi') \tag{18.114}$$

Similarly we obtain for  $T$  with the boundary value  $T(\xi = 0) = 1$  that it is the exponent of an area:

$$T(\xi) = \exp\left(\frac{1}{m_0^2} \int_0^\xi q(\xi')dA(\xi')\right) \tag{18.115}$$

Note that the area element spanned by the vectors  $q$  and (the lightlike)  $dA$  is  $d\Sigma = \sqrt{(qdA)^2 - q^2dA^2} = qdA$ . If we multiply the second of equations (18.113) by  $q$  we also find that  $q$  becomes timelike and its invariant length quickly approaches the value  $m_0$ :

$$dq^2 = 2\left(1 - \frac{q^2}{m_0^2}\right)qdA \Rightarrow q^2(\xi) = m_0^2[1 - T^{-2}(\xi)] \tag{18.116}$$

If we introduce the case when the directrix is built up by finite lightlike parton energy-momentum vectors, then we can construct the quantities  $T$  and  $q$  recursively by

$$T_{j+1} = \frac{T_j}{\gamma_{j+1}}, \quad q_{j+1} = \gamma_{j+1}q_j + \frac{1}{2}(1 + \gamma_{j+1})k_{j+1} \tag{18.117}$$

$$\gamma_{j+1} = \frac{1}{1 + (q_jk_{j+1})/m_0^2}$$

In this way we obtain

$$q_0 = 0, \quad q_1 = k_1, \quad q_2 = \frac{k_2}{2} + \left(k_1 + \frac{k_2}{2}\right) / \left(1 + \frac{k_1k_2}{m_0^2}\right) \tag{18.118}$$

etc. Similarly for  $T$  we have

$$T_0 = 1, \quad T_1 = 1 + \frac{s_{12}}{2m_0^2}, \quad T_2 = 1 + 2\left(\frac{s_{123}}{4m_0^2} + \frac{s_{12}s_{23}}{16m_0^4}\right) \tag{18.119}$$

etc. The largest power in  $T = T_n$  always has the generic form

$$2 \frac{s_{12}}{4m_0^2} \frac{s_{23}}{4m_0^2} \dots \frac{s_{n,n+1}}{4m_0^2} \tag{18.120}$$

This means that

- T1 in general  $\log T$  is a good approximation to the  $\lambda$ -measure and the parameter  $\log(4m_0^2)$  corresponds to the virtuality  $\kappa$  or the resolution power;
- T2 if any of the partons become collinear or soft then the next-order term in  $T$  will take over so that  $\lambda$ , defined in this way, is infrared stable;
- T3 the result in Eq. (18.115) that  $\log T$  is the area between the  $x$ -curve and the directrix provides an intuitive understanding of the relationship between the fragmentation process and the partonic state as described by the directrix. *The string state has a (mean local) lifetime proportional to the region between the directrix and the  $x$ -curve.*

It is possible to find a solution for the vector  $q$ , which we will call  $\hat{q}$ , which is periodic in the same sense as the directrix is periodic. This means that  $\hat{q}_j = \hat{q}_{j+2(n+2)}$ . In this case  $\hat{q}^2 = m_0^2$ . The vector  $\hat{q}$  can to a good approximation be constructed by iterating Eqs. (18.117) a few periods around the string directrix.

We will from now on only work with this periodic  $q$ -vector function and therefore we drop the circumflex notation. The  $x$ -curve is then defined in terms of this periodic  $q$  as

$$x(\xi) = A(\xi) - q(\xi) \quad (18.121)$$

It is not difficult to see that with this definition the  $x$ -curve is everywhere a timelike curve in the sense that its tangent is everywhere timelike.

From Eq. (18.121) we obtain that the vector  $q$  is the tangent of the  $x$ -curve at every point with a length such that it reaches from the  $x$ -curve to the directrix:

$$dx(\xi) = dA(\xi) - dq(\xi) = \frac{qdA}{m_0^2} q \quad (18.122)$$

Finally, it is possible to do exactly the same construction as we have done from the  $q$ -end also from the  $\bar{q}$ -end and to define the corresponding  $q$ -vector and  $x$ -curve in that case.

## 2 Local parton-hadron duality in the Lund model

The  $x$ -curve provides an interesting possibility for describing the average behaviour of the final-state hadron energy-momentum distributions, [48].

Suppose that we use the ordinary Lund fragmentation probabilities to decide upon a distribution of the rank-ordered group of hadrons in the

fragmentation process so that we know the behaviour of the first, the second etc. hadron in rank. In this way we obtain the distributions of an ordered set of (transverse) mass variables.

After that we proceed to obtain an ensemble of partonic states by means of the dipole cascade model as implemented by ARIADNE and we may fragment these states in accordance with the Lund model prescriptions in JETSET. But we may also partition the  $x$ -curve (defined above) for each state into pieces, each with an invariant size corresponding to the mass distribution of the final-state hadrons.

Comparing the results of the two procedures we find that the partitioning of the  $x$ -curves provides a very good description of all inclusive (single-particle, i.e. average) features of the Lund model. In other words, the partitioning of the  $x$ -curves for the multigluon states provides the same inclusive distributions as the production of the multigluon states with Lund fragmentation added in for each state. This is true even if we decide upon a subdivision of all (partonic) states into states with a particular value of  $\lambda$ , a particular value of sphericity etc, [48].

The theory group from Gatchina in the present St Petersburg, [52], have introduced the *hypothesis of local parton-hadron duality* in order to be able to relate their analytical calculations of the partonic-state features (in the LLA and modified LLA) to the final observable hadronic states. They have obtained quite good descriptions of many (inclusive) features of the final states in this way, [52].

The results described above means that there is a direct correspondence in the Lund model. The Lund model results, [48], go even further because as far as we know all inclusive (single-particle) features can be derived from considerations of the  $x$ -curves, which correspond to the properties of the chosen partonic state ensemble. We note, however, that in this scheme with partitioning of the  $x$ -curve the result is not a property of the individual partons. All hadron formations involve at least two neighboring partons so that the final-state hadron makes use of the energy-momentum from at least two partons in order to come onto the mass shell.

The stretching of the curve stems from the color connection between the neighboring partons. The relationship between the  $x$ -curve and the parton energy-momenta is in that way similar to the relationship between a hyperbola and its asymptotes in the form of two lightlike vectors. If any of the partons in a state is collinear or soft the  $x$ -curve in a well-defined sense ignores that parton direction and just continues onwards along the main partonic directions.

It is necessary, in connection with the partitioning above, to decide upon the value of the parameter  $m_0$  which occurs in the defining formulas. We find in [48] that  $m_0$  actually corresponds to a *resolution parameter* along the directrix state. Small values of  $m_0$  correspond to moving close to the

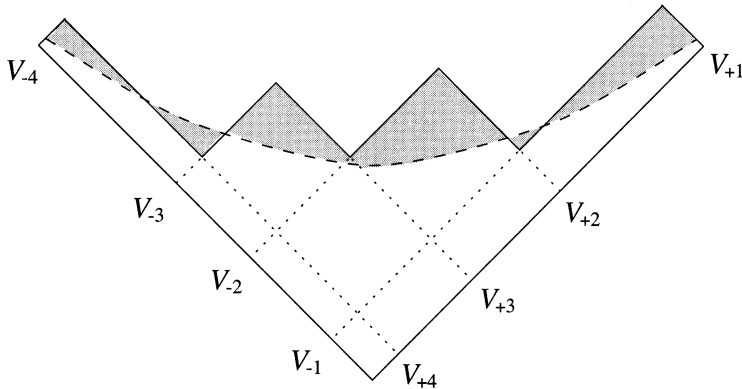


Fig. 18.7. The breakup in a Lund string segment, with the area, the typical hyperbola and the area in between exhibited, together with the characteristic coordinates for the decay.

lightcones while larger values mean that the hyperbolas are less sensitive to the many small fluctuations in a multiparton final state.

The best results are, not surprisingly, obtained if we choose the  $m_0$ -parameter so that it is close to the mean hyperbola in the breakup situation. If, as a theoretical experiment, we change the  $a$ -,  $b$ - and  $\sigma$ -parameters in the Lund model, it turns out that we still obtain a very good description of the final-state hadronic energy-momentum distributions if we adjust the parameter  $m_0$  accordingly.

It is also possible within the same scenario to investigate the fluctuations along the fragmentation cascade in the Lund model. To that end we return to the breakup situation as depicted in Fig. 18.7 for a string segment between two partonic excitations. If we turn the figures discussed in Chapters 7–11 through 90 degrees we obtain the corresponding  $x$ -curve description. We have exhibited both the breakup area and the typical hyperbola (parametrised  $V_+V_- = B$ ), i.e. the correspondence to the  $x$ -curve, together with the area between the two; this ‘in between’ area is shaded in the figure.

In order to calculate the size of the shaded area we note that the part of it spanned by the region  $(V_{+1}, V_{-1})$  is

$$V_{+1}V_{-1} - \int_{B/V_{-1}}^{V_{+1}} \frac{Bdx}{x} - B = B(\rho_{11} - \log(\rho_{11}) - 1) \quad (18.123)$$

where we have used that the hyperbola cuts the line  $V_{\pm} = V_{\pm 1}$  at  $V_{\pm} = B/V_{\mp 1}$ . We have also defined  $\rho_{11} = V_{+1}V_{-1}/B$ .

The next part of the shaded area is below the hyperbola and its size is

easily found to be

$$-\left(\frac{B}{V_{+2}} - V_{-1}\right) V_{+2} + \int_{V_{+2}}^{B/V_{-1}} \frac{Bdx}{x} = B(\rho_{21} - \log \rho_{21} - 1) \quad (18.124)$$

where we have used the same methods as before and defined  $\rho_{21} = V_{+2}V_{-1}/B$ . This area should be subtracted because it corresponds to something lacking from the total. The procedure is now evident and if we define  $\log \rho_{ij} = y_{ij}$  and

$$G(y) = \exp[-bB(\exp y - y - 1)] \quad (18.125)$$

we note that the negative exponential of the area  $AB$  can be written as

$$\frac{G_{11}G_{22}G_{33}\cdots}{G_{21}G_{32}\cdots} \quad (18.126)$$

with  $G_{ij} \equiv G(y_{ij})$ . The meaning of the hyperbolic angles is evident: they correspond to the length along the hyperbola which is spanned by the corresponding coordinates. For small values of  $y$  the function  $G$  may be approximated by a gaussian. We are evidently describing the Lund model breakup process as something rather similar to a Brownian motion along the typical hyperbola. The parameter of this hyperbola is typically  $B = a/b$  in terms of the Lund  $a$ - and  $b$ - parameters.

If we go back to the process for transverse momentum generation (the Ornstein-Uhlenbeck process) which was discussed in Chapter 12, in particular to the Langevin equation

$$\frac{dv}{dt} = -\rho v + R, \quad \frac{dx}{dt} = v \quad (18.127)$$

and compare this to Eqs. (18.113) and (18.121),

$$\frac{dq}{d\lambda} = -q + \frac{dA}{d\lambda}, \quad \frac{dx}{d\lambda} = q \quad (18.128)$$

we notice the strong similarity. In both cases there is a ‘friction term’, corresponding to the fact that it takes some time to turn from one direction to another in the process. The particles in the Lund model are produced one after another, neighbors to some extent keeping close in phase space. We may further identify the ‘time’ variable in the transverse momentum with the  $\lambda$ -measure in the ‘longitudinal’ process. Further, while the longitudinal process is governed by the given directrix  $A$ , the transverse momentum is driven by the stochastic noise term  $R$ , which we may intuitively identify as describing the noise of the soft gluons which drown in the longitudinal process.

Let us finally mention that a correspondence to the Sjöstrand treatment of the Lund model fragmentation has been investigated, [21], as a process along the  $x$ -curve, producing the noise mentioned above. We will not go

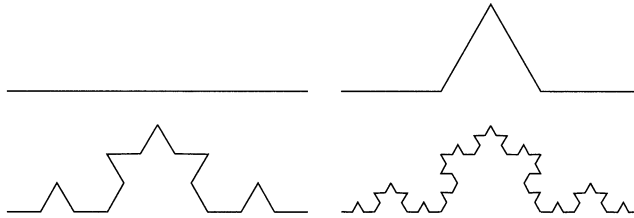


Fig. 18.8. Three generations of the self-similar construction process for the straight-line snow star by von Koch.

into details because the results, although in principal interesting, to a very large degree coincide with the ones obtained from Sjöstrand's gluon fragmentation model described in Chapter 15.

### 18.8 The fractal properties of the QCD cascades

We will end this chapter by exhibiting an intuitively appealing way to describe the properties of the  $x$ -curve and the  $\lambda$ -measure.

We start by considering a so-called fractal curve, the snow star construction of von Koch, Fig. 18.8. This is an example of the 'mathematical monsters' invented and investigated in connection with the mathematical crisis at the end of the last century. The basic question was then to what extent the intuitive notions of continuity and connectedness also meant regularity. The uncomfortable answer is that it is possible in a straightforward way to recursively construct any number of seemingly 'nice' objects, like e.g. one-dimensional continuous curves. As one continues the iterations these curves, nevertheless, tend to 'fill up' the regions around them to the extent that they should no longer be considered as one-dimensional objects. The mathematicians were also able to construct single-point clusters, called Cantor dust, which similarly must be considered as one-dimensional curves, as well as two-dimensional surfaces, which tend to cover parts of the three-dimensional space.

One way to produce such objects is to make use of the notion of *self-similarity*. The construction by von Koch is only one of the simplest and most elegant. You take a continuous line of length 1 and subdivide it into three parts. Then on the middle part you change the straight line segment into an equilateral triangle. From then on the 'new' curve is defined to include the outskirts of the triangle. This means that an object of length 1 has changed into one of length  $4/3$ . Then you repeat the procedure for the four different parts and obtain four new projecting triangles. The new

curve will now have the total length  $(4/3)^2$ . This construction can go on as long as you are able to visualise the procedure and at the  $n$ th step you have a ‘measuring rod’ (i.e. the length of the elementary segments) of size  $\ell_n = (1/3)^n$  to measure the curve length  $L_n = (4/3)^n$ . Note that every part is by construction the same as all others and related to the earlier steps only by a scale change.

Nowadays one defines the *fractal dimension*,  $D$ , as [80]

$$D = 1 - \frac{dL_n}{d\ell_n} = \frac{\log 4}{\log 3} \quad (18.129)$$

Therefore  $D$  is a number between 1 and 2, i.e. the construction leads to something which, intuitively, fills the plane ‘partially’.

When we go back to Fig. 18.1 and the general construction we have presented for the  $\lambda$ -measure and the  $x$ -curve we note that the  $\lambda$ -measure depends upon the size of the ‘measuring rod’, i.e. the size of the  $k_{\perp c}$  at which we stop the construction.

In Fig. 18.5 we have shown what Fig. 18.1 looks like from below. It is easy to see that the many out-sticking branches, twigs and subtwigs which occur in Fig. 18.5 have clear similarities to the construction by von Koch shown in Fig. 18.8. The main difference is that while the von Koch construction is a deterministic process, i.e. every step is completely fixed, the  $\lambda$ -structure is stochastic in nature. Thus every step is determined by a probabilistic scenario. If we use exactly the same considerations that led to Eq. (18.129) in Eq. (18.92), then for the mean value of  $\lambda$  using  $\kappa$  as the measuring rod we obtain

$$D = 1 + \sqrt{\frac{3\alpha_s(k_{\perp}^2)}{2\pi} - \left(\frac{1}{4\kappa} + \frac{3c\alpha_s(k_{\perp}^2)}{4\pi\kappa} + \dots\right)} \quad (18.130)$$

These results would mean that it is possible, using today’s fashionable language to call the quantity  $\langle\lambda\rangle$  a *multifractal* with dimension equal to  $1 + \epsilon$ , where  $\epsilon$  is the *anomalous dimension* of the QCD multiplicity distributions, [52]. The word *multifractal*, [80], is used in order to stress that the dimension is changing with the size of the measuring rod. The result of comparing the first term in Eq. (18.130),  $\sqrt{3\alpha_s}/2\pi$ , to the ARIADNE Monte Carlo, [73], is not a good approximation. The second (negative) term makes it into an essentially better approximation.